Faculty of Mathematical, Physical and Natural Sciences
Department of Materials Science
PhD in Nanostructures and Nanotechnologies

Different functionalization approaches to target micro and nano vectors toword tumor cells

Candidate: Alice Galbiati
Cycle: XXIV: 2008/2011
Supervisor: Prof. Alessandro Desideri

INDEX

1. INTRODUCTION

Nanotechnology is a rapidly-expanding field dealing with the control, manipulation and understanding of matter at scale ranging approximately between 1 and 1000 nanometers (Ferrari, 2005). It has led to the development of a wide ensemble of structures and devices with relevant applications in a variety of fields including, manufacturing, electronics, communication, robotics and medicine (Watson, 2004). Nanomedicine represents the branch of nanotechnology with application to the biomedical sciences and healthcare system (Kim *et al*, 2010; Sahoo *et al*, 2007; Jain, 2010). It concerns the finely tuning of the interaction between a man-created device and a biological system, for applications such as imaging, drug delivery, thermal ablation, clinical diagnostics, biomolecules separation and analysis, cell immunoisolation and analysis (Adiga *et al*, 2009; Huh *et al*, 2007).

1.1 Role of Nanomedicine in cancer therapy

The recent years have witnessed unprecedented growth of research and applications in the area of nanoscience and nanotechnology. There is increasing optimism that nanotechnology, applied to medicine, will bring significant advances in the diagnosis and treatment of disease. Anticipated applications in medicine include drug delivery, in vitro and in vivo diagnostics and production of improved biocompatible materials, suitable as scaffold for tissue engineering (Duncan, 2003; Ferrari, 2005). A device often used consist of engineered nanoparticles (NP), nano-sized particles with adjustable composing material, particle shape, size and surface conjugation, that can be used for therapeutic, diagnostic and imaging purposes (Fadeel *et al*, 2010).

Dispersed NPs, have been used to several aims such as to have fluorescent biological labels (Bruchez *et al*, 1998; Tian *et al*, 2008), to destruct tumors via heating hyperthermia (Shinkaj *et al*, 1999), to deliver drugs and genes (Cui *et al*, 2007; Pantarotto *et al*, 2003), to bio-detect pathogens (Edelstein *et al*, 2000) or proteins (Nam

et al, 2003), to probe DNA structure (Cui *et al*, 2004), to engineer tissues (De la Isla *et al*, 2003; Ma *et al*, 2003), to separate and purify biological molecules and cells (Molday *et al*, 1982), to have magnetic resonance imaging (MRI) contrast enhancement (Weissleder *et al*, 1990) or to carry on phagokinetic studies (Parak *et al*, 2002).

The application of NPs in cancer therapy is limited by the presence of physiological barriers like vascular endothelial pores, heterogeneous blood supply, heterogeneous capillary architecture etc (Jain, 1989; Jain, 2001). In order to have a successful treatment, it is very important to overcome the barriers, and so improve the availability of the drugs. The amount of drug needed to reach the target site and the speed by which the drug can pass the systemic circulation strongly influences the drug bioavailability. In drug delivery it is important to carefully consider the concept of bioavailability, in fact drugs usually have a narrow therapeutic index range and it is easy to remain below the therapeutic threshold, or reach a toxic concentration (Bannon *et al*, 2005). Most of

the drugs used in chemotherapy show characteristics that affect their bioavailability, such as (Lobenberg and Amidon, 2000):

- high lipophilicity and low solubility in body fluids;
- low permeability through biological membranes and tissues;
- dependence of the absorption by facilitated or active transport saturable processes;
- elevated sensibility to hydrolytic enzyme or pH instability.

In light of these considerations, it is important to characterize systems able to increase the solubility of hydrophobic drugs or to modulate the time dependent release of the active principle (Torchilin, 2006). Nano and microstructures can be used as tools able to mask and correct some of the adverse physical and chemical properties of the transported molecule (Moghimi *et al*, 2005).

Nano and microstructures can be properly modified to:

- increase the solubility of poorly soluble drugs in physiological environments;
- protect labile molecules from degradation and chemical inactivation by enzymes;
- increase the bioavailability;
- reduce or avoid side effects.

Hydrophobicity and low solubility in water are intrinsic characteristics of many anticancer drugs (taxanes, tamoxifen, camptothecins, etc..), and nanoparticles may be a useful strategy to overcome these properties (Torchilin, 2007). The use of nano-devices able to increase the drug solubility, preserving at the same time the drug integrity and permitting a modular dosage in the target site represents a fascinating perspective in cancer therapy (Yokogawa *et al*, 1990). Nanotechnology has brought a variety of new possibilities into biological discovery and clinical practice. In particular, nano-scaled carriers have revolutionalized drug delivery, allowing to selectively target drugs on organs, tissues and cells, minimizing exposure of healthy tissues (Bhaskar *et al*, 2010).

1.2 Targeting nano-and micro vectors into solid tumors

The possibility to select molecular target is a key point in the development of strategies able to increase the effectiveness and reduce side effects of anticancer drugs. Considerable progress has been made over the past 2-3 decades in the development of polymeric carriers for a targeted drug delivery to solid tumors (Kopecek *et al*, 2000; Duncan, 2003). The polymeric carriers can be classified as passive or active, depending on their mechanism of targeting.

Polymeric systems, due to their macromolecular nature, passively accumulate in target tissues, such as the reticuloendothelial system (RES) (Gindy and Prud'homme, 2009), through nonspecific uptake by macrophages, or through tumors retention (Matsumura and Maeda, 1986) (Maeda *et al*, 2000), a process called enhanced permeability and retention (EPR). The EPR effect is a characteristic of tumors or inflamed tissues and can be used to target anticancer agents toward cells or tumor tissues (Matsumura and Maeda, 1986). The

enhanced permeability and retention process allow a passive targeting, based on physical and chemical characteristics of the particle, thus not involving a specific recognition between target cell and particle. The EPR effect can be summarized according to the following cascade of events:

- tumor angiogenesis results in hyper-vasculature, providing increased blood flow to the tumor;
- tumor vasculature becomes highly permeable to macromolecules and plasma proteins due to the production of vascular permeability factors, such as bradykinin and tumor necrosis factor;
- the low function of lymphatic drainage, observed in tumors, results in long-term retention of macromolecular drugs.

Nanoparticle's tumor accumulation is due to the highly permeable tumor blood vessels, having large fenestrations, up to a micrometer, as a result of rapid and defected angiogenesis (Figure 1) This effect results in penetration of large carriers in tumors and in a decreased

renal clearance of the delivered structures (Noguchi *et al*, 1998).

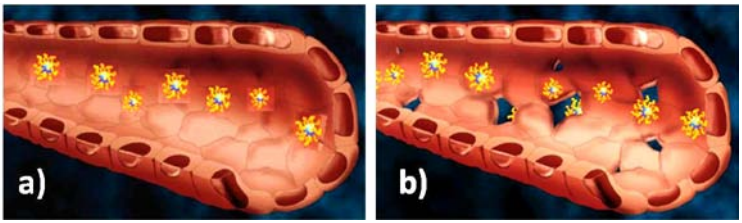

Figure 1. EPR Effect (Enhanced Permeability and Retention). Nanothecnological vectors penetrate through the fenestrated capillary network in pathological tissues interstitium, where they can be potentially degradated, releasing the drug and elevating their local concentration. In A) an healthy capillary with nanoparticles flowing inside. In B) a tumoral vessel whit an alterated architecture (Gindy and Prud'homme, 2009, modified).

Particles with appropriate size, able to remain in circulation for an adequate period of time, can extravasate and passively accumulate in tumor tissues, where the drug can be released from the microstructures. A challenge often overlooked, when using the EPR effect as a rationale for drug delivery, is the elevated interstitial fluid pressure due to the dysfunctional lymphatic drainage that helps the NPs retention (Boucher *et al*,

1990). This factor causes the NPs accumulation in the tumoral area, but also an interstitial hypertension and an impaired blood supply, which reduces convective transport in the core of the tumor (Boucher *et al*, 1990; Jain, 1987). The increase of interstitial fluid pressure reduces the effective transport of anticancer agents in the central area of solid tumors (Jain, 2005).

Active targeting can in part overcome the limitations of drug penetration (Nori and Kopecek, 2005), trough a specific and selective recognition of cancer cells by the engineered structure. Particles, designed to be actively transported, have physical and chemical surfaces properties suitable for a real differential interaction between tumoral and healthy cells and can overcome the limit of the passive drug targeting (Nori and Kopecek, 2005). As an example, Davis and colleagues have shown the tumor localization of gold nanoparticles functionalized with transferrin at variance on what observed for the not functionalized nanoparticles (Choi *et al*, 2009). Similarly, folic acid functionalized micelles are selectively internalized by tumor cells to a greater extent

than the control, made by micelles without folic acid (Lu *et al*, 2009). RGD peptides (Arg-Gly-Asp) have been conjugated to human antibodies (Schraa *et al*, 2002), liposomes (Dubey *et al*, 2004; Koning *et al*, 2004), and poly(ethylene glycol) (Chen *et al*, 2004) to improve the biodistribution and tumor accumulation into tumor cells.

Different type of modification of the nano-and microcarrier allows the structure to be actively transported:

- chemical conjugation of molecules that specifically recognize and bind to receptors or ligands over-expressed on cancer cells surfaces, like antibodies (Zaman *et al*, 2011), folic acid (Chen *et al*, 2011) and transferrin (Huang *et al*, 2011; Han *et al*, 2010);
- polymers that respond to local stimuli, characteristic of the pathological area, such as changes in pH (He *et al*, 2011), temperature or chemical variation, pH sensitive disulphide bonds (Kennet *et al*, 2007), or temperature

sensitive polymeric structures (Geng *et al*, 2011);

- cell penetrating peptides that fuse directly with cell's plasmatic membrane, avoiding the passage in the endosomes and preventing the lysosomal degradation, or polymers and peptides with a buffering endosome function and escape like PLL (poly-L-lysine) and PEI (poly ethylene imine) (Fu *et al*, 2011; Neu *et al*, 2005).

An active transport, based on carrier's chemical modification, requires knowledge of the targeting molecule and makes crucial the concept of particle's architecture.

1.3 Nano and microsystems architecture for drug delivery

Rapid advances in nanotechnology has permitted the incorporation of multiple therapeutic, sensing and targeting agents into nanoparticles (for example, liposomes, viruses and quantum dots), with a size ranging from 1 to 1,000 nm (Ferrari, 2005). These agents

are offering new possibilities for detection, prevention, and treatment in oncology (Rakesh *et* al, 2010). The use of nanoparticles gives the possibility to create a carrier which binds one or multiple drugs that can be directed against cancer cells or tumor microenvironment, permitting tumors visualization and simultaneously enhancing drug-circulation times. Another important property concerns the controlled drug-release kinetics that allows a superior dose scheduling for improved patient compliance (Torchilin, 2007; Schroeder *et al*, 2010; Wagner *et al*, 2006).

Over 20 nanoparticles have been approved by the FDA for clinical use (Zhang *et al*, 2008; Davis *et al*, 2008). Nanoparticle formulations for the treatment of solid tumors include liposomes (such as pegylated liposomal doxorubicin and liposomal daunorubicin), albumin-bound paclitaxel, polymeric particles (such as methoxy-PEG-poly[D,L-lactide] taxol) and many formulations that are in preclinical and/or clinical trials (Zhang *et al*, 2008) (Table 1).

Table 1. Representative examples of marketed nanoparticle-based drug delivery and imaging contrast agents

Commercial name	Carrier type	Active agent	Benefit
Doxil® Caelyx®	PEGylated liposome	Doxorubicin	HIV-related Kaposi's sarcoma (Northfelt *et al*, 1998)
Myocet®	Liposome	Doxorubicin	Metastatic ovarian cancer (Gradishar et *al* 2005)
DaunoXome®	Liposome	Daunorubicin	HIV-related Kaposi's sarcoma (Gill *et al*, 1996)
Onco TCS®	Liposome	Vincristine	Relapsed aggressive non-Hodgkin's Lynphoma (Gindy and Prud'homme, 2009)
Abraxane®	Albumin	Paclitaxel	Metastatic Breast cancer (O'Brien *et al*, 2004)

Tab 1: Examples of nano-and microstructures for cancer therapy that passed all the clinical trials and are already on the market (Gindy and Prud'homme, 2009 modified).

Although less toxic than conventional therapies, these agents are still associated with adverse effects, such as steatites and palmar–plantar erythrodysesthesia for pegylated liposomal doxorubicin (Gordon *et al*, 2001) and sensory neuropathy and nausea for albumin-bound paclitaxel (Gradishar *et al*, 2005). For these reasons it is crucial to develop new systems. The design of a new

carrier for drug delivery is an engineering process that must consider all the physical barriers, defining the best vector architecture to reach the target (Torchilin, 2006). Most of the microstructures for biomedical uses present a tripartite basic structure (Ferrari 2005) (Figure 2)

I. **Outer shell:** It may contain antibodies or ligands aimed at recognizing cancer cells surfaces, or protective molecules like polyethylene glycol (PEG) that prevents the interaction between the particles and the reticuloendothelial system (RES), responsible of the particles clearance (Huynh *et al*, 2009).

II. **Core:** It is the bulk material that composes the particle. It can be organic or inorganic, but it must be biocompatible. It is used as basis for the chemical synthesis of the external shape or as scaffold for drugs adsorption.

III. **Inner shell:** It may contain drugs or contrast agents, covalently or not covalently bound, or can be part of the core (Cho *et al*, 2008).

In the following section I will describe some successful nanosystems, some of which have been used during my thesis work.

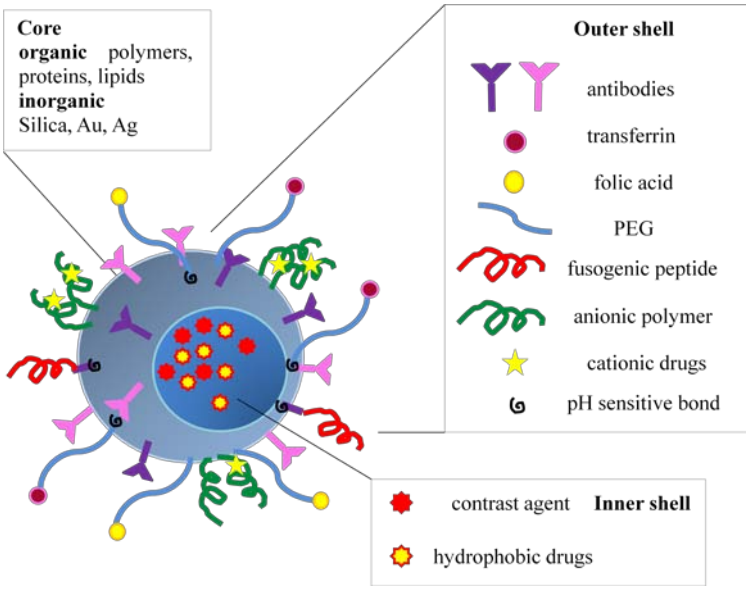

Fig 2: Hypothetic tripartite architecture of nanoparticles useful for cancer therapy.

1.3-1 Liposomes

The nano and micro-devices in the market (Table 1) belong to the class of colloids made by a solid phase

suspended in a mobile phase. Liposomes belong to this class and are widely used due to their versatility and ease of preparation (Masserini *et al*, 2002). Liposomes have been developed in 1965 by Bangham, as simplified models for cell membranes (Bangham *et al*, 1965; Bangham *et al*, 1965; Bangham, 1993). Today are used as carriers of molecules in different areas: genetics (Mel'nikova *et al*, 1999), engineering (Clark *et al*, 1999), chemotherapy (Sachdeva, 1998; Nguyen *et al*, 2011; Ferraretto *et al*, 1996), immune-modulation (Scott and Groot, 2010), and cosmetics (Suntres, 2011). Liposomes are mainly made by phospholipids and sterols found in nature, so their toxicity is extremely limited and possess an excellent biocompatibility (Torchilin, 2007; Masserini *et al*, 2002). The liposomes diameter can vary from 50 nm to some micron; they can incorporate lipophilic molecules in the phospholipids bilayer and encapsulate hydrophilic compounds in the aqueous core. The liposomes are easily functionalized and generally are conjugated with PEG, which provides an hydrophilic outer shell, able to increase the blood circulation time,

limiting the interaction with proteins (long-circulation liposomes) (Torchilin, 1998).

1.4 Poly-vinyl alcohol microbubbles and microcapsules.

Poly-vinyl alcohol (PVA) is a water-soluble polymer, biocompatible and injectable, which can be used as a basis to produce various microstructures, such as hydrogel-based PVA structures for tissue reconstruction (Bakhashancleh *et al*, 2011), PVA films for drug delivery application (Padula *et al*, 2007) and PVA microbubbles filled with gas as contrast agent (Wheatley and Lewandowski, 2010).

Microbubbles (MB) and microcapsules (MC) are soft matter devices used in several applications ranging from protein separation and purification to ultrasound imaging (Cavalieri *et al*, 2005). PVA-MB are polymeric spherical structures, ranging in size between 2μm and 4mm, filled with air or other specific gases, that can be used as contrast agents (Lencioni *et al* 2002). PVA-MCs are produced from MB in presence of ethanol, that replaces

the air inside the bubbles, giving rise to the MC. The surface is characterized by the presence of free-OH groups, that provide water solubility and reactive aldehyde groups, that can be used to functionalize the microstructures (Cavalieri *et al*, 2006). On the microcapsules surface, pores having a size range between 3.5 and 6.5 nm are present. Diffusion of molecules of different size trough the microcapsules shell suggests that the shell architecture is characterized by a cross-linking density gradient, with large pores at the polymer/solution interface and small ones at the air/polymer interface (Figure 3) (Cavalieri *et al*, 2005).

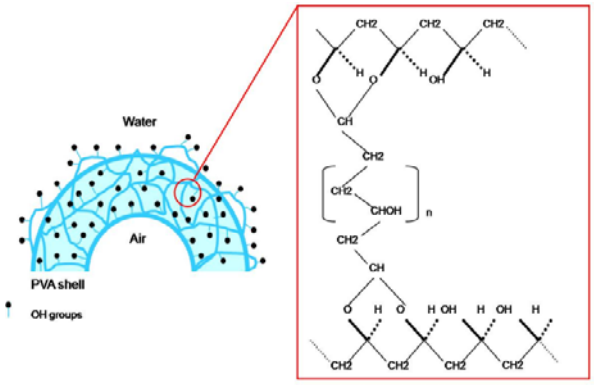

Fig 3: PVA network in MC/MB. Chemical bonds between different PVA molecules (Galbiati et al, 2010).

The structures are able to trap different type of molecules, due to the double nature of PVA, having hydrophobic and hydrophilic component made by vinyl groups and OH- groups respectively. In Table 2 are reported some physical characteristics of MC and MB measured at 37°C.

Table 2. Structural Parameters of PVA Microbubbles and Microcapsules Obtained at Room Temperature

	External diameter (μm)	Internal diameter (μm)	Shell thickness (μm)
Microbubbles	*5±1 a,b*	*3±1 a*	*1± 0.9 a*
Microcapsules	*6±1 a,b*	*4±1 a*	*1± 0.9 a*

a Confocal laser scanning microscopy. b Dynamic light scattering.

Tab 2: Some physical characteristics of MB and MC obtained at room temperature (Cavalieri et al, 2005 modified).

MBs are widely used as contrast agents in ultrasounds clinical tests, due to their high biocompatibility and injectability. They can amplify the gray scale signal

obtained during the normal echography. Contrast specific imaging techniques permit enhancement of ultra sounds (US) agents in gray-scale, with optimal contrast and spatial resolution and offer high sensitivity either to microbubbles movement or to microbubbles destruction, depending on the level of the applied acoustic peaks pressure (Lencioni *et al*, 2002). MB facilitates the US-deflection and reflection of ultrasonic waves, that is only slightly scattered by body fluids, providing an interesting strategy for amplify the US-scattering (Hernot and Klibanov, 2008). MB can be also used as carriers to deliver drugs, small molecules, nucleic acids and proteins, that can be delivered in a specific site where the cargo can be released inducing the MB explosion through an intense use of US (Tinkov *et al*, 2009). MB, when scanned through a low peak pressure (0-100KPa), behave as linear backscatterers, but when the incident peak pressure increases (100kPa to 1MPa) MB show nonlinear characteristics and emit harmonics able to amplify the echographic signal. At high acoustic peak pressure, destruction becomes the most important phenomenon

that provides an amplified signal, proportional to the MB concentration (Harvey *et al*, 2001; Dalla Palma and Bertolotto, 1999).

PVA-MBs are produced from PVA chains of different lengths of a constituent unit $(CH2\text{-}CHOH)_n$. Figure 4 shows the chemical structure of atactic PVA, a polymeric chain with a base unit connected as head to head or head to tail. The atactic PVA is converted in telechelic PVA, to allow the formation of PVA-MB, trough oxidation of the head to head bonds. The reaction occurs in water solution in presence of sodium meta-periodate (a strong stereo specific oxidant) and modifies the PVA-chains terminals, leaving two aldehydic reactive end groups (Figure 4). The amphiphilic nature of PVA permits the formation of an organized network of telechelic PVA at the air-water interface. The OH groups are preferentially in contact with the water solution while the carbon main chains are exposed to the external air. A homogenization process at the air-water interface allows the peculiar organization in spherical structures containing air in the internal compartment (Cavalieri *et al*, 2006).

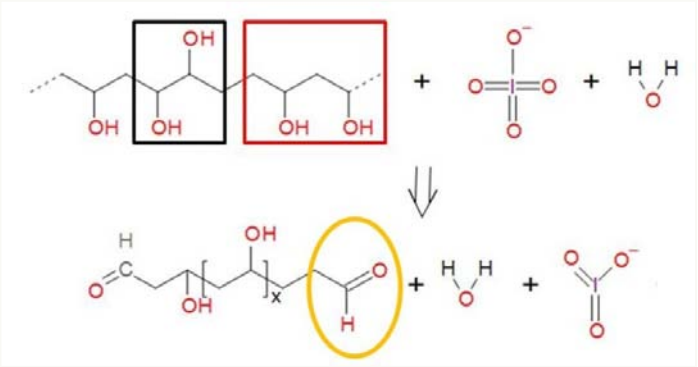

Fig 4: oxidation of telechelic PVA (top), made up of repeating units of head / head bonds (red box) and head / tail bonds (black box) to atactic PVA. Only-head/head (red box) units are subject to stereospecific oxidation by sodium meta-periodate (NaIO4). This reaction create some aldeidic terminals (yellow circle).

1.5 Silica nano-particles.

Silica nanoparticles can be easily produced due to the aqueous chemistry of silica. The occurrence of the neutral monosilicic acid Si(OH)4 is limited in diluted aqueous solutions ([Si]100 ppm) at room temperature and in neutral or moderately basic media (2≤pH<9±10) . At high pH values, the formation of silicate anions $SiO(OH)^-_3$ and $SiO2(OH)^{2-}_2$ occurs (Bases and Mesner, 1974; Selvan *et al*, 2010). The increase of silicic acid

concentration leads to the formation of dimeric species. The first condensation reaction involves a nucleophilic substitution (SN_2) of a Si-OH oxygen atom with another silicon atom, that leads to the formation of a Si-O-Si siloxane bond, and to the loss of a water molecule (Coradin and Lopez, 2003):

$$Si(OH)_4 + HO\text{-}Si(OH)_3 \longrightarrow (OH)_3Si\text{-}O\text{-}Si(OH)_3 + H_2O$$

Generally, the hydrolysis and condensation occur simultaneously (Bases and Mesner, 1974). The process may start between two neutral species, but the reaction is very slow. Trimer, tetramer and oligomer formation proceeds in a similar manner (Figure 5). The substitution, in these oligomers, of a Si-OH group with a Si-O-Si siloxane linkage increases the charge of the silicon atoms that become more electrophilic and constitute a preferential site for further monomer addition.

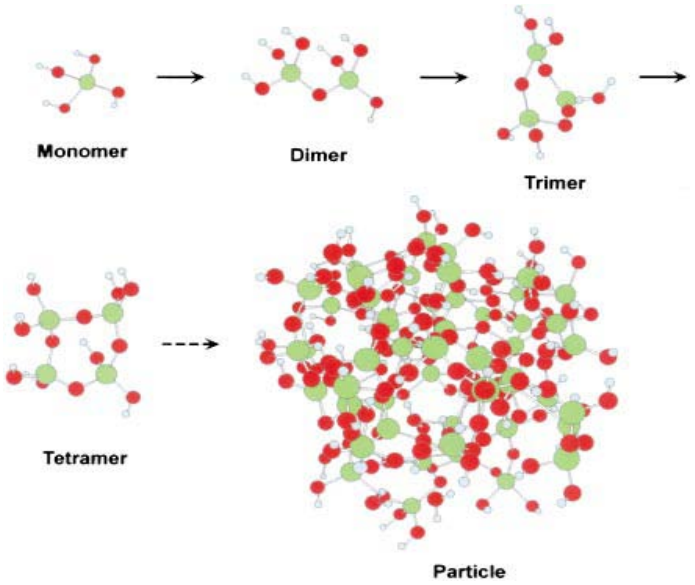

Fig 5:. Polymerization behavior of silica. In acid aqueous solution monosilicic acid condenses to form dimeric, trimeric, and tetrameric (Likely cyclic) structures, which effectively then evolves to form particles with sizes in the nanometer range.(Coradin and Lopez, 2003).

In the absence of salts or other additives, the production of the initiation nuclei is dictated by pH. At pH values below 7, particles aggregate because only weak electrostatic repulsions exist.

Steric and electrostatic characteristics of the particles permit the elongation of the chain, resulting in a fibrillar

assembly. The chain can also elongate laterally, producing a three-dimensional open network having large water-filled cavities (gel; Figure 6). At pH values above 7, the electrostatic interactions between charged particles limit the aggregation process, so the particles increase in size and decrease in number and the solubility decreases upon size increasing (sol; Figure 6) (Coradin and Lopez, 2003).

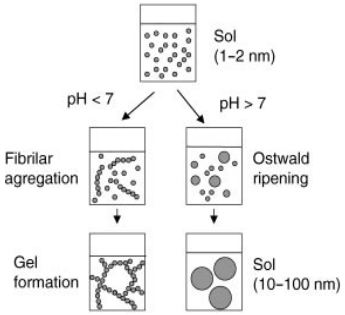

Fig 6: Sol-gel formation processes. At pH 7, the initial particles undergo fibrillar aggregation, which effectively leads to gel formation. At pH7, the ostwald ripening process leads to the growth of larger particles, which effectively can form a stable sol.at pH values above 7 (Coradin and Lopez, 2003).

The process is named sol-gel synthesis and can be modulated since it is influenced by pH, salt and temperature.

The condensation of O-Si-O network can occur also in presence of modified monomer having a general formula

R'-Si$(OR)_3$. In this case the hydrolysis rate is influenced by the nature of the alkyl R'-group, decreasing upon increasing the steric hindrance of R' (Deng *et al*, 2009).

Stöber and Fink have introduced a method for modifying the sol-gel synthesis starting from a tetraethylorthosilicate (TEOS) monomer in ethanol solution and ammonia, that gives rise to spherical particles with an highly controlled size (Tabatabaei *et al*, 2006). The Stöber particles can be considered pure silica, infact in TEOS the R' group is an OR group and the polymerization takes place in the four directions corresponding to the four bonds of the Si atom.

In their general formula the alcohoxisilicate derivative can polymerize in three directions and the non hydrolyzble R' group that is still linked to the silicon, confers an organic nature to the structure. The particles are called organically modified silica nanoparticles (ORMOSIL) (Roy *et al*, 2005)

Using specific stabilizers such as cetyltrimethylammonium bromide it is possible to produce mesoporous nanoparticles, useful for drug

delivery due to their ability to encapsulate drugs in the mesoporous network (Liu *et al*, 2011). Other type of silica structures can be generated using single and double emulsion. In this case it is possible to have particles with an external shape of silica and an internal compartment containing water or oil. The emulsion technique offers the possibility to encapsulate different compounds. In my thesis work I have focused my attention on silica oil in water microemulsion, a system that is produced in aqueous environment, where the DMSO oily phase is dripped slowly in presence of surfactants and co-surfactants. The micellar hydrophobic components autoassemble in water in little drops, which constitute nano-reactors for the silica shell's assembly (Roy *et al*, 2005).

Varying the composition of surfactants and their concentrations it is possible to obtain micelles with different diameter and stability, while changing the composition of the different precursors it is possible to obtain silica particles with different surface chemical properties (Liu *et al*, 2011).

Aerosol-OT is used as surfactant and butanol as cosurfactant to produce the amino functionalized silica nanopartcles (NH_3-ORMOSIL). The oily phase is constituted by DMSO that is left to drip slowly into the solution. The nanoparticle shell is produced using two silica precursors:

1) **vinyl-triethoxysilane (VTES)** has an hydrophobic vinyl group as R'-group, that preferentially interacts with the oily component of the emulsion, keeping the alcoholic groups exposed to water.
2) **aminopropyl-triethoxysilane (APTES)** that has an amino propylic group as R'-group, that allows the formation of an outer water soluble shell. The APTES alcoholic groups form covalent bonds with the alcoholic groups of VTES from the bottom layer, while the ammine remains exposed to the polar aqueous solvent (Roy *et al*, 2005).

In Table 3 it is reported the effect of concentration of the micellar system components on nanoparticle diameter.

Composition and size of various ORMOSIL nanoparticles

Aerosol-OT (gr)	nBuOH (μL)	Water (mL)	DMSO (μL)	VTES (μL)	NH3 (μL)	APTES (μL)	Diameter (nm)
0.33	600	20	100	200	20	—	10–15
0.33	600	20	100	200	—	20	10–15
0.44	800	20	100	200	20	—	15–20
0.44	800	20	100	200	—	20	15–20
0.44	800	20	100	200	—	40	15–20
0.44	800	20	100	300	20	—	25–30
0.44	800	20	100	500	20	—	40–45
0.66	1200	20	100	200	20	—	40–45
0.66	1200	20	100	300	20	—	65–75
0.88	1600	20	100	200	20	—	80–8

Tab 3: The table shows the concentrations of surfactant and co-surfactant used to produce silica oil in water micro-emulsions of various diameters (Roy et al, 2005 modified).

During the past few years, organically modified silica (ORMOSIL) nanoparticles have been widely used as DNA carriers for gene delivery (Roy *et al*, 2005; Bharali *et al*, 2005), drug carriers in photodynamic therapy (PDT) (Roy *et al*, 2003; Ohulchanskyy *et al* 2007) and fluorescent probes for tumor visualization (Kim *et al*, 2007) (Kim *et al*, 2007). ORMOSIL nanoparticles can encapsulate fluorophores or PDT drugs and have many important properties:

- the presence of porous structures can facilitate the controlled release of encapsulated biomolecules like drugs and proteins (Roy *et al*, 2003; Ohulchanskyy *et al*, 2007);
- the functionalization of the surfaces with various chemical groups;
- a low cytotoxicity and good biocompatibility (Shimada *et al*, 1995);
- the inner shell may contain hydrophobic drugs such porphyrines, that can be used for PDT therapy, because the porphyrins generate radicals able to escape from the silica shell and explicate their function;
- the possibility to contain either hydrophilic or hydrophobic drugs/dyes permits to ORMOSIL nanoparticles to have a tunable photoluminescence that spans the entire visible and IR spectrum (Burns *et al*, 2006).
- the presence of a positive surface charge gives the possibility to interact with plasmid DNA, a

property that can be used in gene therapy (Roy *et al*, 2005).

Due to the ultra-small size and surface charge, ORMOSIL silica nanoparticles can be non-specifically uptaken by cells through the EPR effect. Bio-molecule-conjugated ORMOSIL nanoparticles offer the possibility to have a new platform to specifically target cancer cells for diagnosis/therapy applications (Jun *et al* 2008).

1.6 Chitosan based Nanopaticles.

Chitosans are a family of binary polysaccharides derived from the deacetylation of chitin, a natural polymer found in nature primarily in the exoschelethon of arthropods and in some fungi. It is a linear polysaccharide composed of randomly distributed β (1-4) glycoside bound between N-acetyl glucosamine and D- glucosamine. (Ribeiro *et al*, 2009). Chitosan structure and consequently its physical properties can be varied by changing the degree of acetylation of the glucosamine monomers, or changing its molecular weight. In its crystalline form, chitosan is normally insoluble in aqueous solutions at pH > 7, but it

becomes soluble at acidic conditions, due to the presence of protonable amino groups on the glucosamine group.

The polymer is non toxic upon its oral administration to humans (Schipper *et al*, 1996). It has been approved as a food additive and incorporated into a wound-healing product (Illum, 1998). Chitosan has also antimicrobial properties (Dai *et al* 2011) and finds application in food conservation (Moradi *et al*, 2011). Chitosan is biocompatible and biodegradable, which makes it ideal as scaffold molecule for drug delivery (Ribeiro *et al*., 2009). It is used in oral (Shelma and Sharma, 2011; Singh *et al*, 2011) and pulmonary administration (Ungaro *et al*, 2011) due to its mucoadhesive properties. Its interaction with epithelial cells and the overlying mucus layer provides a long contact time, useful for the drug transport across the nasal membrane before the formulation is cleared by the mucociliary clearance mechanism (Illum, 2003). Studies in Caco-2 cells revealed that chitosan increases the paracellular transport of polar drugs by transiently opening the tight junctions between epithelial cells (Artursson *et al*, 1994). The most

important application of chitosan is in gene therapy, being a biocompatible alternative to the use of synthetic cationic polymers such as poly(ethylene imine) (PEI) in RNA interference and plasmidic DNA transfection (Köping-Höggård *et al*, 2001, Mao *et al*, 2010). Since 1998 with the discovery of RNA interference (RNAi), the gene therapy has become a powerful tool for treatment of a variety of diseases such as genetic disorders, viral diseases, and cancer. Gene silencing *in vitro* is quite efficient and reliable, but not *in vivo* due to enzymatic degradation, rapid clearance from the blood and poor cellular uptake of RNAi (Higuchi *et al*. 2010). Therefore, drug delivery systems, that protect the nucleic acid from degradation and facilitate their cellular uptake, are indispensably for a successful use of gene therapy *in vivo* (Shim and Kwon, 2010). Chitosan-nucleic acid nanoparticles are relatively easy to produce, since under slightly acidic conditions the aminic groups of chitosan are protonated allowing electrostatic interactions with the negatively charged phosphate groups of nucleic acids (Liu *et al*. 2007). It is possible to define the N/P ratio of

the complexes as the ratio between the amines of chitosan and phosphates of nucleic acid, considering that for N/P=1 the complex is uncharged. Chitosan/nucleic acid nanoparticles facilitate RNAi/pDNA delivery. The complexation also protects the nucleic acid against nuclease degradation (Kim and Kim 2009). The size ranges between 50-300 nm and the net positive charge of chitosan/nucleic acid nanoparticles results in interactions with the negatively charged cellular surface and facilitate their cellular uptake by endocytosis (Liu *et al*. 2007)

1.7 Folic acid (FA), and folate receptors mediated targeting.

Folic acid (FA, folic acid) is an essential cofactor for metabolic reactions such as the synthesis of nucleotides and of some amino acids (Williamson, 2001) and it is present in all the body tissues. Cells use several strategies for the FA transport. One concerns the presence of the reduced folate carrier (reduced-folate carrier, RFC), a membrane protein present in two isoforms of 38 and 44 kDa, which shows low affinity (in the micromolar range)

for folate (Antony, 1992). Folic acid can be also transported via a specific receptor FR (folate receptor) that binds folates in the nanomolar range (Kamen *et al*, 1991). The first two carriers do not have affinity for folic acid conjugates or folic acid functionalized nanoparticles, while FR is able to bind and allows the endocytosis of various types of structures functionalized with FA (Sudimack and Lee, 2000).

Three isoforms of the human folic acid receptor have been identified. The three genes are located on chromosome 11. The α (257 a.a.) and the β (255 a.a.) isoforms have 70% sequence identity, and a marked difference in the tissue specific expression. Both isoforms are membrane-associated with a GPI-anchor (glycosyl-phosphatidylinositol) and are localized in membrane rafts. The γ isoform (243 a.a.) is a soluble placentar protein involved in exchanging folates between mother's and fetal blood (Shen *et al*, 1994). The α isoform is absent or have a low degree of expression in healthy tissues with the exceptions of liver, thyroid, choroid plexus, placenta and kidney (Shen *et al*, 1994)

Ross *et al,* 1994). A large number of epithelial tumors, as the naso-pharyngeal carcinoma cells (KB) and several others, show over-expression of the α isoform (Table 4). The β isoform is over-espressed in tumors of epithelial origin such as sarcomas and leukemia (Ross *et al,* 1999). The FR is often used as a diagnostic marker for ovarian (Coney *et al*. 1991; Miotti *et al,* 1995) and brain cancer (Weitmann *et al,* 1994). The over-expression seems to be related to uncontrolled proliferation. Folic acid is required for nucleotides synthesis and it is necessary to enhance its uptake when cells undergo a rapid division, (Low and Kularatne, 2010).

The role of the over-expression of FRs, in cancer, is not fully clear (Sudimack and Lee, 2000). Cervix carcinoma cells, transfected with the FR's cDNA, results in a decreased proliferation, suggesting that the expression of FR does not provide a proliferative advantage to cells in rapid division (Sun *et al,* 1995).

Other studies have shown that high levels of RF are associated with the aggressiveness of ovarian cancer, as monitored by the increased presence of cells in S phase

Cells/tissues	Determinants	Expression
Normal	Genitourinary system	Placenta, chorionic villus, trophoblastic cells; fallopian tube, uterus, ovary ; vas deferens, epididymis, semen ; kidney (proximal tubules) (Weitman et al, 1992)
	Central nervous system	Choroid plexus epithelial cells, CSF (Holm et al ,1991),
	Hematopoietic system	Hematopoietic progenitor cells [CFU-GEMM. CFU-GM, BFU-E, CFU-E] (Antony et al, 1991)
	Gastrointestinal system	Salivary (submandibular) (Weitman et al, 1992); colon (Holm et al, 1994)
	Respiratory system	Bronchial glands and alveolar lining (type-I and-I1 pneumocytes) (Weitman et al, 1992) .
	Endocrine systems	Breast (acinar cells) (Weitman et al, 1992) and human milk (Antony, 1992); thyroid, pancreas (Weitman et al, 1992)
	Miscellaneous	Fibroblasts (Antony, 1992)
Malignant	Consistently high and uniform expression	Nasopharyngeal carcinoma (Antony, 1992); cervical carcinoma (Sun et al, 1995); ovarian carcinoma (Garin-Chesa et al, 1993); choriocarcinoma (Prasad et al, 1994)
	Relatively lower, inconsistent expression	Endometrial carcinoma (Antony, 1992); primary brain tumors (Weitman et al, 1994); colorectal carcinoma (Garin-Chesa et al, 1993) sarcomas (Ross et al, 1994); renal cell carcinoma (Garin-Chesa et al, 1993)

Tab 4: Folate receptor FR) expression in normal and malignant human tissues

and an increased resistance to the chemotherapy (Toffoli *et al*, 1997). Cancer targeting with folic acid (FA) is a widely used approach, because the over-expression of FRs is typical of many tumor cell lines (Laemon *et al*, 1991; Gabizon *et al*, 2004). The strategy has been

successfully applied to various types of nanocarriers such as liposomes loaded with either daunorubicin (Ni *et al*, 2002) and doxorubicin (Pan *et al*, 2003). Monoclonal antybody (eg MOv18) have been also used to target FR (Sudimack and Lee, 2000). Folic acid functionalized nanoparticle's uptake did not require the partecipation of RFC (Antony, 1992). Independent data from a variety of models, including transplacental folate transport (Henderson *et al*, 1995), cloning of RFC cDNA (Dixon *et al*, 1994) and transfection of RFC-defective cells with FR cDNA (Dixon *et al*, 1992; Spinella *et al*, 1995) have reached similar conclusions. However, data from Kamen and Anderson's group, spawned the concept of linkage of FR and the RFC/(anion channels) in a process called photocytosis (Antony, 1996). The proposed model for receptor-mediated uptake is based on immune-fluorescence experiments that localize FR in membrane domain named caveolae. Caveolae are invaginations in the plasma membrane and are distinct from classic clathrin-coated pits, that are involved in receptor-mediated endocytosis (Anderson, 1993; Anderson *et al*,

1992). In this model, folate binds to GPI-anchored FR that then moves into caveolae able to internalize folic acid. Folate dissociates from its receptor by acidification of the cellular compartment and is transported into the cytoplasm via anion channels simporter. Apo-FR is recycled on cell's surface to bind more folate. A series of consideration support this model:

- the folic acid uptake is inhibited by probenecid, suggesting that an anion channel is involved in the trans-caveolar translocation process (Kamen *et al*, 1991);
- the activators of protein kinase C inhibit the internalization of folate and reduce the number of caveolae (Antony *et al*, 1991);
- low cholesterol concentration inhibits FR-mediated folate transport, due to disruption of integrity of the caveolae (Chang *et al*, 1992).

Additional experiments have questioned the role of caveolae in FR-mediated folate uptake (Anderson, 1993) (Anderson *et al*, 1992). This controversy is based on the evidence that FR accumulation into discrete clusters is

dependent on cross-linking reaction with secondary antibody (Mayor *et al*, 1994). An independent support comes from the necessity of an H+ gradient for cystoplasmatic release of folate (Prasad *et al* 1994). Studies on transcellular folate transport exclude the presence of anion channels, thus, it is plausible that FR may interact with non-RFC H+ pump (Kamen *et al*, 1991).

A new model is based on the FR localization in endocytic compartments named GEECs (GPI-anchored protein enriched endocytic compartments) (Sabharanjak *et al*,2002). GEECs are internalized by an actin-mediated process and are able to engulf also the external fluid phase during the internalization process. This aspect makes GEECs distinct from early sorting endosomes and similar to pinocytic compartement. Formation of GEECs appears specifically regulated by the Rho family GTPase, Cdc42 (a key regulator of actin polymerization), but not by other members or the same family such as RhoA and Rac1, infact only the loss of Cdc42 function inhibits the fluid phase uptake via the GEECs (Sabharanjak *et al*,

2002). The FR localization into GEECs is supported by the following findings:

- replacement of the FRs GPI-anchor by transmembrane domain of the LDL induces the co-localization of FRs with TfRs (transferrine receptor), known to be internalized by clathrin coated endosomes (Sabharanjak *et al*, 2002);
- the inhibition of clathrin coated endosome uptake by potassium depletion has not effect on the FR internalization (Sabharanjak *et al*,2002; Benmerah *et al*, 1999);
- expression of negative dominant Cdc42 severely compromises the internalization of FR-α into GEECs.

The mechanism for folic acid internalization by FR can be summarized in the following steps (Figure 6):

- folic acid interacts with the FR present in the GEEC;
- The GEEC is closed to form a membrane vesicle that also contains the extra-cellular fluid phase;

- The internalized GEEC migrates into a perinuclear compartment called REC (recyling endocytic compartement);
- The GEEC's acidification via H+/pump causes the detachment of folic acid from its receptor;
- Folic acid can be released into cytosol in symport with a proton by a FA/H+ transporter.
- The GEEC is recycled in membrane where it is able to bind additional folic acid (Sabharanjak *et al*, 2002).

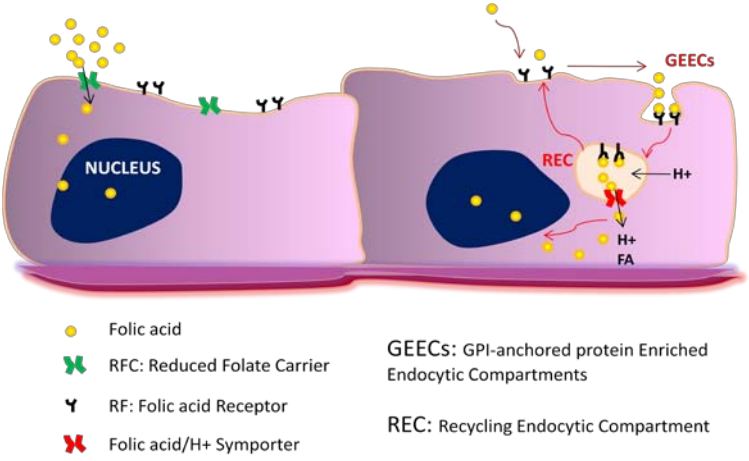

Fig 6: Most reliable model for folic acid receptor internalization pathway.

1.8 DNA topoisomerase IB (TopoIB)

Type IB topoisomerases fall into two highly related but separated structural categories. The first one includes the viral TopoIB, exemplified by vaccinia topoisomerase I (v-topo I). The second one includes the eukaryotic enzymes, typified by the well-studied human topoisomerase I, human TopoI (Leppard and Champoux, 2005). The ability to relax DNA supercoils allows these proteins to play an essential role during replication (Yang *et al*, 1987), transcription (Gilmour and Elgin, 1987), recombination (Bullock *et al*, 1985) and chromosome segregation (Maul *et al*, 1986).

TopoIB can relax the positive supercoils that accumulate ahead of the movement of polymerases. The catalytic cycle of TopoIB consist of (Figure 7):

- Binding to DNA (Figure 7A)
- A trans-esterification reaction between the hydroxyl group of a tyrosine residue, placed at the active centre, which provides a transient covalent bond with the 3´end of the cleaved strand (Figure 7B-C)

- Relaxation of DNA that is propelled by the superhelical tension (Figure 7D)
- Resealing of the phosphodiester bond using the energy stored in the DNA-TopoIB complex (Figure 7E-F)
- Releasing of DNA, restoring the integrity of the double helix (Figure 7G).

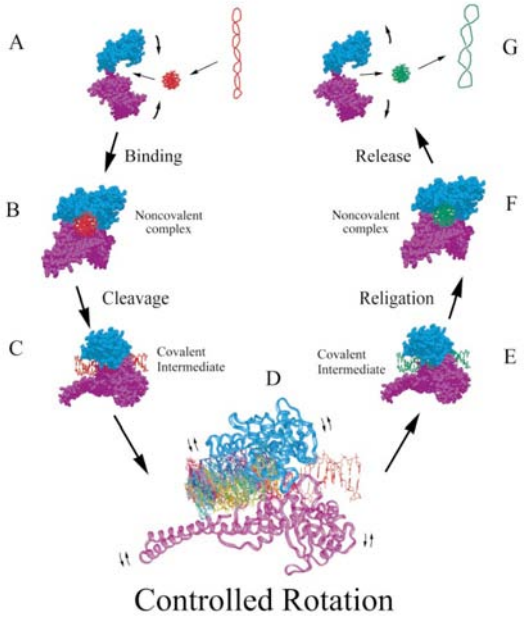

Fig 7: Controlled rotation mechanism of human topoisomerase IB, as an example for TopoIB family (Stewart *et al*, 1998).

The energy of the phosphodiester bond is conserved in the protein-DNA covalent intermediate and so the cleavage-religation step does not require ATP hydrolysis. TopoIB are ubiquitous in eukaryotes, where they represent the major DNA topoisomerase I activity. Two different TopoIB are present in vertebrates, one localized in the nucleus and the other in the mitochondria (Zhang *et al*, 2004). Eukaryotic TopoIB are large monomeric enzymes (around 90 kDa) with a highly conserved DNA binding domain and a C-terminal catalytic domain, linked by a non conserved hydrophilic region. Based on conservation of sequence, sensitivity to limited proteolysis, X-rays analysis and fragment complementation experiments (Stewart *et al*, 1997) the 91-kDa human TopoIB protein has been divided into four distinct domains (Figure 8):

- an N-terminal domain (a.a. 1-214) that is poorly conserved, highly charged, protease sensitive, unstructured (it was not possible to crystallize it) and not required for activity in vitro. The

domain contains five nuclear localization signals (Mo *et al*, 2000);

- a highly conserved core domain (aa 215-635) that contains all the residues forming the active site (Arg488, Lys532, Arg590, His632) excluding the catalytic tyrosine (Tyr723). It is divided into three subdomains: Subdomains I and II (Figure 8, yellow and blue)form a 'cap' over bound DNA, contributing to a pair of α-helices, termed the 'nose cone'. The cap is connected to the core subdomain III (Figure 8, red) by a short hinge helix, whereas core subdomain III (Berger and Schoeffler, 2008);
- a protease sensitive and poorly conserved linker domain (aa 636- 712) that is positively charged and organized into two long α-helices (α18 e α19) that form a coiled-coil structure that protrudes from the base of the enzyme (Figure 8, orange);
- a conserved C- terminal domain (aa 713-765) that contains the catalytic tyrosine (Tyr723)

organized into five short α-helices (Figure 8, green). The Tyr723 is located on the loop connecting α-helices 20 to 21 and its mutation to phenylalanine inactivates the enzyme (Redinbo *et al*, 1998).

The core and C-terminal domain form a clamp that encircles DNA in a positively charged central hole of 20 Å. The surface of the cavity hosts several positive charged residues that interact with the negative charged surface of DNA.

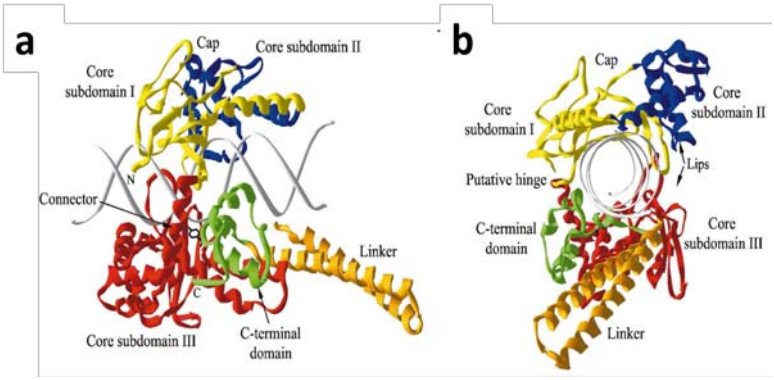

Fig 8: Two visions of the structure of non-covalently bound DNA to human TopoIB. (a) The structure of the enzyme observed from the side with the axis oriented perpendicularly to DNA (b) longitudinally (Champoux, 2001).

1.9 The camptothecin structure and mechanism of action.

The camptothecin (CPT) is an alkaloid extracted from barks, wood and fruits of *Camptotheca acuminate*, an Asian plant member of the Nyssaceae family. The drug is part of the quinolone family having an indole monoterpenoide structure (Wall *et al*, 1966) (Figure 9).

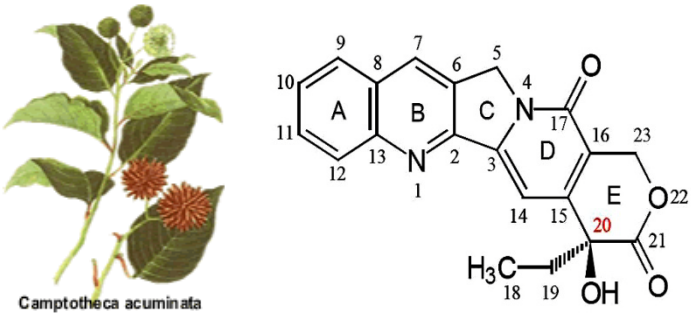

Fig 9: Image of *Camptotheca acuminata* and chemical structure of camptothecin. In figure is shown the planar shape of CPT that is constituted of five rings named from A to E (Wall *et al*, 1966).

Since the 60s has been noted that the extract of *Camptoteca acuminata* had antibacterial, anticancer and antiviral properties. In the 80s it has been demonstrated

that CPT is the active principle, and that its molecular target is topoisomerase IB (Hsiang *et al*., 1985) The drug is poorly soluble in water and several studies have been focused on the characterization of new derivatives more soluble and more appropriate for clinical use (Ulukan and Swaan, 2002).

CPT has a skeleton structure composed of five rings that comprise two quinoline rings (rings A and B) two interposed rings (C and D), and a terminal α-hydroxy-δ-lactone ring with a chiral center in position C-20 (E) (Figure 9) (Wall *et al*., 1966). CPT is present in nature in the form 20 (S) which is able to inhibit the topoisomerase I activity 100 times better than the 20 (R) isomer (Garcia-Carbonero and Supko, 2002), indicating that the interaction between the drug and the enzyme is stereo-specific.

The planar configuration of the five rings is essential for the inhibition of human TopoI. The chemical reactivity of the E ring is another key point since the ring undergoes a spontaneous reversible hydrolysis, that opens the ring at neutral or alkaline pH, giving rise to the soluble

carboxylated form. Under physiological condition the soluble carboxylated form is the predominant one, while the active lactone form is predominant at acidic pH values (Fassberg and Stella, 1992; Pizzolato and Saltz, 2003) (Figure 10). In some acidic districts of the human body, such as the bladder, the carboxylic acid is converted into the less soluble lactone, resulting in severe side effects such as hemorrhagic cystitis. For these reasons, CPT is not used in the treatment of cancer, but the use of the soluble derivatives irinotecan and topotecan is preferred.

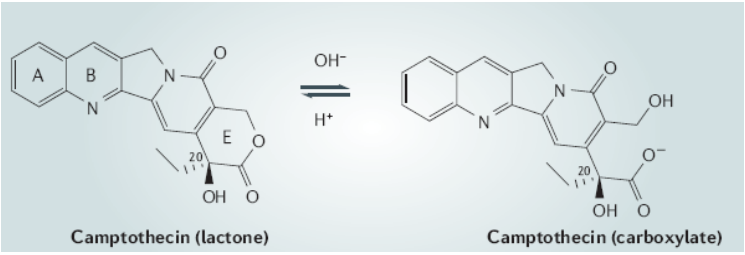

Fig 10: Dynamic equilibrium of CPT between lactone and carboxylated form (Pommier, 2006).

Irinotecan, that has an antitumor activity lower than CPT, is currently in use in the treatment of colorectal cancer (Pizzolato and Saltz, 2003). It is a prodrug that is converted in vivo into its active metabolite, SN38 (Takasuna *et al*, 1996). Topotecan, in addition to the increased solubility in water has a cancer killing activity comparable to camptothecin and it is approved by FDA (Food and Drug Administration, USA) for the treatment of ovarian cancer (Kingsbury *et al*, 1991). Other derivatives of CPT are esatecan and rubitecan. Esatecan is an esacyclic derivative with increased activity, compared to CPT, TPT and SN38, on gastric, pancreatic, liver, ovarian and colorectal cells. It is currently under clinical trial. Rubitecan is insoluble and acts as a prodrug being converted in vivo into an active metabolite. It is usually administered in liposomes formulation via aerosol, to increase its tolerability in patients with hepatocellular carcinoma (Zheng *et al*, 2011).

Camptothecin inhibits the enzyme by stabilizing the human TopoI-DNA cleavable complex, decreasing the rate of DNA religation (Hsiang *et al*, 1985). The drug

doesn't bind to free topoisomerase (Leteurtre *et al*, 1993), but reversibly intercalates between bases +1 and -1 of the cleaved DNA, stabilizing the TopoI-DNA covalent complex (Tanizawa *et al*, 1993). The complex itself is not harmful, but during cell division the stalled complexes can collide with the DNA replication machinery causing a double-strand break and cell death via apoptosis (Strumberg *et al*, 2000; Pommier, 2006). For this reason the drug works when the cells are in the S phase of the cell cycle (O'Connor *et al*, 1991). Tumor cells are more sensitive than healthy cells, due to their fast division (Liu *et al*, 2002).

2. AIM OF THE PROJECT

Micro and nanoparticles have been recently exploited to tackle two important points in medicine namely: drug specific targeting and gene therapy. In my thesis I have covered both aspects although concentrating a large part of my work on the first one.

In detail as far as the drug specific targeting is concerned, I have used the strategy of folic acid functionalization using as micro and nano-carriers poly-vinyl alcohol microcapsules (PVA-MCs) or organically modified silica nanoparticles (ORMOSILs). PVA-MCs show high versatility, biocompatibility (Cavalieri *et al*, 2006) and a three-dimensional water soluble network able to adsorbs different chemical compounds. In my thesis I have studied the delivery of camptothecin (CPT), a powerful and insoluble antineoplastic drug, adsorbed on PVA-MC. The microparticles have been functionalized with folic acid using two different linking procedures. In one case a chitosan-folate complex has been produced and then linked on MC surface. Chitosan has been used as spacer arm to allow a varied three-dimensional orientation of the

folate group. In the other case MCs have been functionalized with lysine, that is then used to link folate. This modification permits to functionalize the particles with a large number of folic acid molecules. The systems, tested for localization and viability on epithelial tumor cell lines and on a healthy connective line, have been shown to display a strong preference for the tumor cells.

The strategy of folate-mediated active targeting has been also applied to a system of silica-based nanoemulsion (ORMOSIL). The resulting FA-ORMOSIL has been tested for the FR-mediated localization in tumor cell lines, showing that the internalization process is not totally determined by FR.

As far as gene therapy is concerned I have explored the possibility to use chitosan as biocompatible carrier for plasmid DNA. Chitosan is a natural, biocompatible polymer that can interact with nucleic acids to form a transfectable nanoparticle. Aim of my work has been to clarify the suitability of some already known chitosan derivatives in macrophages transfection. Macrophages cell lines are difficult to be transfected, but the possibility

to have macrophages cell lines stably transfected with a therapeutic gene can open huge possibility in cancer treatment. My experiments indicate that the ultra-pure chitosan derivatives produced by Novamatrix, that are considered to be powerful transfecting agents, are not able to grant the expression of the plasid in J477A-1 murine macrophage cells. The work has been done during a six months period in the Jørgen Kjems laboratory in the molecular biology department of the Aarhus University in Denmark.

3. MATERIALS AND METHODS

Instruments.

High-resolution ^{1}H NMR spectra were recorded on a Digital NMR Spectrospin AVANCE 300, Bruker. Chitosan and chitosan_folate 3 mg/mL are dissolved in D_2O with 3 % v/v CD_3COOD solution, using tetramethylsilane (TMS) as the internal standard. The release kinetics of the drug were performed using Perkin-Elmer Lambda 2 UV/vis double beam-spectrophotometer. Fluorescence microscopy images were obtained with the DeltaVision system (Applied Precision, Washington, USA) equipped with an Olympus inverted microscope IX 70. The image workstation includes SoftWoRx software for digital image acquisition, deconvolution, and optical sectioning.

Dynamic light scattering, DLS, measurements distribution of the different type of MC were carried out with a BI-200SM goniometer (Brookhaven Instrument Co.), equipped with a solid state laser source at 532 nm. The correlation functions were collected at 90 degrees

and data analysis was carried out with standard Brookhaven software package using the CONTIN algorithm. Z-potential measurements were carried out with a MALVERN Zetasizer apparatus equipped with a 5 mW HeNe laser. Low applied voltages were used to avoid the risk of effects due to Joule heating.

The AFM measurements were performed using a home designed microscope from Istituto di Struttura della Materia - CNR, Rome, Italy, described in (Cricenti and Generosi, 1995) this instrument, can operate under controlled environmental conditions. The AFM measurements were performed in air, at room temperature and constant 30% relative humidity.

Materials.

All solvents and reagents were of analytical grade and were used as received. Poly vinyl alcohol (PVA) was obtained from Sigma Aldrich. Number average molecular weight determined by membrane osmometry was 30 000 (5000 g/mol). Weight average molecular weight, determined by static light scattering, was 70 000 (10 000 g/mol). Low molecular weight (50 kDa) chitosan, 75-

85% deacetylated, rhodamine-β-isothiocyanate, sulfo-rhodamine B, (S)-(20)-camptothecin, 95% HPLC, Triton X-100, folic acid, dimethyl sulfoxide (DMSO), (3-aminopropyl)triethoxysilane (APTES), vinyl triethoxysilane (VTES), Aerosol-OT, lysine, 1-butanol, Huron tetrafluoroborate (TBTU), Idrossibenzotriazolo (HOBT) and Diisopropyl-ethylamine (DIPEA) were Sigma products. Sodium periodate, and inorganic acids and bases, used for telechelic PVA preparation and microballoon synthesis and modifications, were RPE products from Carlo Erba.

Cell culture media were obtained from Gibco. Alexa-488-conjugated phalloidin, alamar blue, were obtained from Molecular Probes. Lipofectamine, Lipofectamine 2000 were obtained from Invitrogen. Ultrapure chitosan oligomer O15, O25 and G214 Novafect pDNA Kit were Novamatrix products.

GFP encoding Plasmid DNA:……

<u>Reagents for the synthesis of Poly-vinyl alcohol MB / MC</u>

- (PVA, poly-vinyl Alcohol) (Sigma-Aldrich, 89.000 to 98.000 AM)
- Distilled water (ddH2O)
- Sodium meta-periodate (Sigma, 213.89 p.m.)

Reagents for functionalization and labeling of MB / MC

- Rhodamine-β-isothiocyanate (Sigma-Aldrich, Mw 536.1) dissolved in dimethyl sulfoxide (DMSO, Sigma-Aldrich, Mw 78.13) to a final concentration of 3 mg/ml, the resulting solution is stored at 4 ° C in the dark (being a fluorophore, the rhodamine is photosensitive)
- Chitosan 50 kDa, 75-85 % deacetylated (Sigma-Aldrich)
- D-Lysine (Lys, Sigma-Aldrich, Mw 146.19.)
- Sodium cianoboroidruro (NaBH3CN, Sigma-Aldrich, Mw 62.84)
- Low molecular weight (50 kDa) chitosan, 75-85% deacetylated
- Folic acid (FA, Sigma-Aldrich, Mw 441.4)
- Huron tetrafluoroborate (TBTU, Sigma-Aldrich, Mw 321.08)

- Idrossibenzotriazolo (HOBT) (Sigma-Aldrich, Mw. 135.12)
- Diisopropyl-ethylamine (DIPEA) (Sigma-Aldrich, Mw 129.25)

Reagents for chitosan nanoparticles production

- Chitosan 100kDa, 100% deacetylated (Chitopharm)
- Ultrapure chitosan oligomer O15, O25 and G214 100% deacetylated Novafect (Novamatrix)
- Cy3 labeled 50 kDa chitosan was given by S. Hein from the department of molecular biology of the Aarhus University of Denmark, characterized to have 0.4 % of NH_3 groups of chitosan substituted with Cy3
- GFP- plasmid DNA was given by J. B. Bramsen from the molecular biology department of Aarhus University of Denmark
- Cy3 labeled GFP plasmid DNA was given by J. B. Bramsen from the molecular biology department of Aarhus University of Denmark

-30mM acetate buffer pH 5.5

-ddH_2O nuclease free

Oil/Water microemulsion production

- dimethyl sulfoxide (DMSO, Sigma-Aldrich Mw 78.13)
- (3-aminopropyl)triethoxysilane (APTES, Sigma-Aldrich, Mw 221.37)
- vinyl triethoxysilane (VTES, Sigma-Aldrich Mw 190.31)
- Aerosol-OT (Sigma-Aldrich, Mw 444.57)
- 1-butanol (Sigma-Aldrich, Mw 74.12)

Oil/Water microemulsion functionalization

- Folic acid (FA, Sigma, Mw 441.4)
- Huron tetrafluoroborate (TBTU, Sigma-Aldrich, Mw 321.08)
- Idrossibenzotriazolo (HOBT, Sigma-Aldrich, Mw. 135.12)
- Diisopropyl-ethylamine (DIPEA, Sigma-Aldrich, Mw 129.25)

Drug solutions

- Camptothecin (CPT, Sigma-Aldrich, Mw 348.35) dissolved in DMSO to a final concentration of 4mg/ml (11.8 mM), the solution is stored at -20 ° C in the dark as a photosensitive drug.

Cell lines

- HeLa, human tumor cell line of cervical cancer. It's a cell line formed by cancer cells of epithelial origin.
- H1299, human lung cancer cells. It is a cell line tumor of epithelial origin
- NIH-3T3, murine embryonic cell line. It's consists of a cell line connective tissue fibroblasts cells.
- J774A-1, murine macrophage cell line

Soils and nutrients for cell cultures

- RPMI1640 (Eurobio)
- DMEM (Dulbecco's Modified Eagle Medium, Eurobio)
- Antibiotics Penicillin and streptomycin (Eurobio)
- L-glutamine (Eurobio)
- Calf serum (FCS, fetal calf serum) with inactivated complement (Euroclone)
- RPMI1640 (-) FA (GIBCO)
- RPMI1640 (-) Phenol Red (Eurobio)

Immunofluorescence localization experiments

- 3.7% paraformaldehyde in PBS 1X, 1X Prepared by diluting 37% paraformaldehyde in PBS solution (Sigma-Aldrich, PM 30.03)

- blocking solution: 3% BSA, Tween-20 0.05% in 1X PBS (Sigma-Aldrich)
- 0.1% Triton in PBS 1X, 1X Prepared by diluting in PBS Triton X-100 (Sigma-Aldrich)
- Primary antibody antiFRα (Bioworld Technology)
- Secondary antibody labeled with rhodamine isothiocyanate-β-(Alexafluor 555) (Jackson ImmunoResearch), diluted in Blocking Solution: 3% BSA, 0.05% Tween-20 in 1X PBS;
- Phalloidin-FITC (Alexafluor 488, Invitrogen-Molecular probes);
- Upright (DPX MOUNTANT for histology, Sigma-Aldrich);

Assay of cell viability with Alamar Blue ®

- Alamar Blue (Molecular Probes) diluted 1:10 in DMEM or RPMI1640 medium (depending from the cell line) supplemented with 10% FCS, 1% LGlutammina, 1% antibiotics penicillin / streptomycin.

Assay of cell proliferation with sulfo-rhodamine B (SRB)

- SRB 0.4% in acetic acid 1% (Sigma-Aldrich Mw 577.11)

- Trichloroacetic acid 40% (TCA, Sigma-Aldrich)
- Acetic acid 1% (Sigma-Aldrich)
- Tris-base 10mM pH 10.5

Solutions and Buffers

Phosphate Buffer Saline (PBS) (1 L, 20X, pH 7.4). Prepared by:

- 160 g sodium chloride (NaCl, Eurobio, Mw 58.44)
- 4 g of potassium chloride (KCl, Sigma-Aldrich, Mw 74.56)
- 28.8 g sodium phosphate (Na2HPO4, Sigma-Aldrich, Mw 177.99)
- 4.8 g of potassium dihydrogen phosphate (KH2PO4, Sigma-Aldrich, Mw 131.1)

The reagents are dissolved in distilled water (ddH2O) and the solution is adjusted to pH 7.4 by adding HCl fuming 12M.

Methods.

Cells culture

HeLa cells (immortalized human cell line derived from cervical cancer) and NiH3T3 (mouse embryonic fibroblast cell line), were grown in D-MEM (Dulbecco Modified Eagle Medium) with 10% Fetal Calf Serum (FCS) 100 U/mL penicillin, and 0.1 mg/mL streptomycin.

H1299 (a human non small cell lung cancer derived from lymph node) and J774A-1 (murine macrophage cell line) were cultured in RPMI-1640 (Roswell Park Memorial Institute) with 10% Fetal Calf Serum (FCS) 100 U/mL penicillin, and 0.1 mg/mL streptomycin, and maintained in humidified atmosphere of 5% CO_2 at 37 °C. Cells were harvested twice a week and used at about 80% confluence.

Synthesis of PVA-coated microbubbles and conversion into microcapsules

Synthesis of telechelic PVA was previously described (Paradossi *et al*, 2003) (Paradossi *et al*, 2002). Stable (air-filled) PVA-coated microbubbles were prepared by cross-linking telechelic PVA at the water/air interface. Briefly Dissolve 4 g of PVA in 200 ml of distilled water

at 80 ° C, in a glass beaker on a magnetic stirrer, until the solution becomes clear. Add 380 mg of sodium meta-periodate to allow the oxidation of the head-head hydroxyl groups of PVA into aldehydic groups (thus becoming telechelic PVA, as shown in figure 4); Keep stirring for one hour at 80 ° C.

Than vigorous stirring at room temperature for 2 h by an Ultra-Turrax T-25 at 8000 rpm equipped with a Teflon coated tip generated a fine foam of telechelic PVA acting both as colloidal stabilizer and as air bubble coating agent. This procedure allows the telechelic PVA to organized at the air/water interfaces and to close, after omogenization, in circular structures containing air (microbubbles, MB). microbubbles were separated from solid debris and extensively dialyzed against Milli-Q water.

The aqueous suspensions of microbubbles were obtained and used for microcapsule preparation: PVA microbubbles were converted into solvent-filled microcapsules by equilibrating an aqueous suspension in ethanol 70% solution. The microcapsule suspension was

then extensively washed by a series of centrifugations at 1000 g to remove ethanol excess.

Synthesis of Chi-Rod

Chitosan 0.5% (w/v) was suspended in 100 mL of acetic acid 3% (v/v) solution. 50 mg of rhodamine-β-isothiocyanate was then added and stirring maintained for 48 h in the dark at 4 °C (Qaqish and Amiji, 1999). The solutionwas adjusted to pH9 with NaOH, and unreacted rhodamine-β-isothiocyanate was removed carrying out at least 5 centrifugation steps at 1000g for 10 min. The synthesized compound was extensively dialyzed against Milli-Q-water.

Synthesis of chitosan-folate (Chi-FA) and chitosan-folate-rhodamine (Chi-FA-Rod) complexes

1.2 mmol of EDC (N- (3-dimethylaminopropyl)-N0-ethylcarbodiimide hydrochloride) were added to 3 mmol of FA dissolved in 50 mL of DMSO, and left to react for 1 h in the dark at roomtemperature. Then, 50 ml of a 1% (w/w) chitosan or chitosan_rhodamine in 20 mM acetate buffer pH 4.7 was added to the reaction. After 16 h, the solution was brought to pH 9 with NaOH, and the

compound purified by centrifugation followed by 3 days of dialysis against acetate buffer and extensive dialysis against Milli-Q water using a 12 kDa cutoff dialysis membrane. The compound was then freeze_dried.

Preparation of chitosan (MC-Chi) and chitosan-folate (MC-Chi-FA) functionalized microcapsules.

Chitosan was conjugated to microcapsules by reductive amination. Chi or Chi-FA was dissolved in a sodium acetate 0.2 M, acetic acid 0.3Mbuffer at pH4.5 to a concentration of 0.15% (w/v). A 10 mL sample of 1 mg/mL microcapsule aqueous suspension was added with 4 μL of Chi or Chi-FA solution at room temperature. The pH was carefully adjusted to 5.0 with acetate buffer, following the addition of $Na(CN)BH_3$. The resulting suspension was stirred for 1 day at room temperature. The microcapsule suspension was then extensively dialyzed and washed to remove low molecular weight reaction products and unreacted chitosan.

Preparation of lysine functionalized microcapsules (MC-Lys)

1mg/ml solution of MC reacts with a big excess of Lysine (0.5 mg) for 2 hours room temperature, following the addition of 1mg/ml $Na(CN)BH_3$ for stabilize the shiff base between Lysine-NH_3 and the aldeydic moiety of PVA-MC. The sodiocianoboroidruro, being a reducing agent, allows the formation of an amide bond between PVA and lysine, that is more stable than a Schiff base

Lysine functionalized MC (MC-Lys) are purified by a series of centrifugations 1000 g in water and quantified.

Preparation of folic acid-lysine functionalized microcapsules (MC-Lys-FA)

Folic acid is linked to lysine-NH_3 via coupling reaction and formation of an amide bond between the two carboxylic groups of FA and the free amino group of lysine. To facilitate the reaction is necessary to increase the reactivity of carboxylic acid, turning it into an activated ester. For this purpose are generally used a class of coupling reagents:

- Huron tetrafluoroborate (TBTU)
- Idrossibenzotriazolo (HOBT)
- Diisopropyl-ethylamine (DIPEA)

The last one is a base that has the role of removing the protons formed during the condensation between carboxyl and amino groups. This reaction is weighted on the amino groups of lysine used in the MC-Lys production and the amount of folic acid used during the reaction. In particular:

- 2 equivalents (eq) of folate (respect to lysine NH_3) were dissolved in ddH2O.
- 1.2 equivalents of. TBTU were added in respect to the carboxylic groups of folate (taking in consideration that each folate molecule has two carboxylic groups).
- 1.2 equivalents of HOBT in respect of each carboxyl group of folate.
- 2.4 equivalents of DIPEA (olways in respect to the carboxylic groups).

The reaction was leaved in stirring for 10' at room temperature in the dark (folate is sensitive) to enable the formation of the activated ester on folic acid molecule, then was added the amine (ie MC-Lys) and let stir for 24 hours, room temperature in dark, in order to obtain MC-Lys-FA.

The day after MC-Lys-FA were washed 5 times in ddH2O centrifugation at 1000 g for 10 'in order to eliminate the excess of unbound FA. Due to the low folic acid solubility in water, the functionalized MC were transferred in dialysis tube (cut-off from 12.000 to 14.000) and dialysed against ddH2O for 24h and then quantified.

Rhodamination of PVA-MC

Suspensions of 1 mg/mL of MC were added with 10 μL of rhodamine-β-isothiocyanate 40 solution 2.3 mg/mL in DMSO and stirred for 1 h. The rhodamine excess was removed by at least 5 centrifugation steps at 1000g for 10 min, changing the external medium.

Folic acid quantification on MC surface

The amount of folic acid conjugated is quantified measuring the absorbance of MC-Lys-FA dissolved in 1M NaOH, subtracting the absorbance of a MC-Lys solution at identical concentration, The folic acid quantification is obtained using the ε_{FA} in NaOH 1M (ε_{FA} =9500 $M^{-1}cm^{-1}$) and tha absorbance at the maximum of the spectrum (364 nm).

Particle size distribution of PVA-MC

Size distribution of microcapsules was evaluated by dynamic light scattering, DLS. MilliQ water are used as dispersing medium for the analysis. For these measurements, a BI-200SM goniometer (Brookhaven Instrument Co.), equipped with a laser source at 532 nm, was used. The correlation functions were analyzed with CONTIN algorithm.

Adsorption of the CPT on different type of functionalized MC and evaluation of drug release kinetics

CPT in DMSO solution 11.8mM were added to a 1 mg/mL suspension of functionalized MC, until a final concentration of 100 μM and stirred for 4 days in the dark.

Then, three washes were performed by centrifugation at 1000 g to remove the drug that was not adsorbed. The concentration of drug in the washing is calculated by spectrophotometer following the absorption at λ = 370 nm (corresponds to the maximum absorption of camptothecin). The percentage of adsorbed CPT on microcapsules was indirectly estimated by subtracting the

total concentration of drug present in the wash to the total drug used for the adsorption. A suspension of functionalized MC 1 mg/mL (20 mL), previously adsorbed with CPT 100 μM, was resuspended in different kind of medium (water, PBS, (D-MEM) without phenol red, with or without 10% fetal calf serum (FCS) and glutamine), and subdivided into 20 aliquots of 1 mL. The MC aliquots were kept in an incubator shaking at 140 rpm, 37 ºC. At different times, the samples were centrifuged for 5 min at 2000 g and the supernatant was read spectrophotometrically at λ = 370 nm.

Absorption values were fitted with the equation:

$$A = Amax[1 - \exp(Kt)]$$

to estimate the time constant of the kinetics (K^{-1}) and maximum release Amax.

Adsorption/release experiments with different CPT concentrations

1mg/mL of MC, MC-Chi and MC-Chi-FA are equilibrated in CPT solutions at different concentrations of drug for four days. After three washings, the amount of loaded CPT is determined as explained in the above

section. Release was accomplished by equilibrating the microcapsules in renewed MilliQ water or in PBS at pH 7.4 to a volume of 1ml. The amount of released drug from differently coated microcapsule was determined as described in the above section. Every three days the external medium is replaced and the drug released is expressed as a percentage of the total absorbed on the microstructures.

Microcapsule localization experiments

For fluorescence studies, cells were grown in Lab-Tek chamber slides (Nunc Inc.) in RPMI-1640 medium without folate and treated with MC, MC-Chi, and MC-Chi-FA in RPMI with or without folate as described previously. After 48 h of incubation, cells were washed, fixed with 3.8% paraformaldehyde solution in phosphate buffered saline, and permeated by using 0.1% Triton X-100. In case of MC, MC-Lys and MC-Lys-FA cells were seeded in normal medium for 24 h and medium were changed 30´ befor adding the trectaments using RPMI-1640 medium or RPMI-1640 (-) FA medium. Cells were fixed and permeated 24 h later. Actin filaments were

labeled by using Alexa-488-conjugated phalloidin according to the manufacturer's instructions. Fluorescent signals were detected and photographed using a Delta Vision 3.0 microscope. To assess the direct involvement of folate mediated interaction, localization experiments have been carried out also in the presence of free folate. After 48 h of culture in folate-free medium, MC-Chi-FA were given to cells in either folate-free or folate-supplemented medium (final concentration 4 mg/L). Cells were fixed and stained after the 2 day treatment and localization assays were performed as described.

Cell culture and proliferation assay

For proliferation studies, cells were detached with trypsin/EDTA for 5 min and centrifuged. Cells were resuspended in RPMI-1640 medium without folate and seeded in 96-well culture dishes ($2.5 \cdot 10^3$ cells per well) and left grow for 48 h. After this time, medium was refreshed and cells were incubated for additional 48 h with MC, MC-Chi, and MC-Chi-FA (either adsorbed with CPT or not), and 24 h with MC, MC-Lys and MC-Lys-FA (with or without CPT). At the end of incubation,

medium was refreshed again, and after 48 h, the percentage of cell proliferation was evaluated by the sulforhodamine assay (Papazisis *et al*, 2008) or the alamar blue® assey, calculating the values as a percentage of the control, considered to be 100%. Proliferation assays were also carried out by cell counting using a Neubauer modified chamber. In this case, cells are seeded in 12-well culture dishes at $7.5 \cdot 10^3$ cells per well. This protocol was established in order to discriminate between the antiproliferative effect due to the diffusion of CPT released from the microcaplules in the media and the one due to the direct cell_microcapsule interaction.

Sulfo-rhodamine assey

After treatment with different type of structures the medium was aspirated and cells were washed with PBS. Cells were then fixed with cold 40% TCA for 1 h at 4 °C. The TCA was removed and cells washed 5 times with ddH2O and left to dry.

SRB 0.4% acetic acid were added 50 µL of for 30 min at room temperature. Then was aspirated and cells washed again for 5 times with 1% acetic acid and left to dry.

100 µL of 10 mM Tris-base per well were added and left stirring for 5 min, and the absorbance at 492nm was read. The sulfo rhodamin B binds covalently to the surface protein and its concentration at the end of the assay is proportional to cells number.

Alamar blue® assey (resazurin assey)

After treatement cell medium was removed and substituted with medium conteining 10% v/v of alamar blue® solution. Cells were placed in the incubator at 37 °C and 5% CO_2 for 30´. The fluorescence was read with multi-plate spectrophotometer reader using excitation 560 nm and emission 590 nm filter settings.

Resazurin is a non-fluorescent indicator dye that is converted to bright red–fluorescent Resorufin, via the reduction reactions of metabolically active cells. The amount of fluorescence produced is proportional to the number of living cells.

Synthesis of oil/water microemulsions (ORMOSIL-NH_3)

The amino functionalized silica emulsion was product according with the published protocol for producing particles with 20 nm of diameter (Roy et al, 2005).

20 mL of ddH_2O were placed in a backer under high magnetic stirring. Then 0.44 g of Aerosol-OT and 800 µL of 1-butanol were added to the mix and left until everything was dissolved. 100 µL of DMSO (with or without 5mM rhodamine β-isothiocianate) were dropped slowly in to the micellar system and stir for 30´. Later 100 µL of VTES were added, to produce the first silica layer on the emulsion, and left for 1 h. amino-functionalyzed silica nanoparticles were produced adding 20 µL of APTES. The reaction was carried on for 24 h followed from four days of dialysis in tube (cut-off from 12.000 to 14.000) against ddH2O, concentrated using AMICON centrifugal device and then quantified with the dried weight technique.

Synthesis of folic acid modified ORMOSIL nanoparticles (ORMOSIL-FA)

Folic acid was linked to ORMOSIL-NH_3via a coupling reaction procedure using 4 equivalents of folic acid in respect to the number of APTES moles used in the ORMOSIL-NH_3 production. Folic acid was activated in presence of respectively 1.2, 2.4 and 1.2 equivalents of

TBTU, DIPEA and HOBT in respect to the number of folic acid COOH groups.

In particular FA (11.4 mg) was dissolved in 5 ml water adding under magnetic stirring. 19.9 mg of TBTU, 21.2 µL of DIPEA (δ=0.755 g/mL) and 9.5 mg of HOBT for 10´ room temperature, in order to allow the ester activated formation. At last was added the ammine component, the ORMOSIL-NH_3 (20 mg in 20 ml of water as final volume) and keep stirring in dark for 24 h.

The ORMOSIL-NH_3 used for the synthesis were purified after 2 days of dialysis in order to minimize the differences between the two types of structure. The emulsion was than dialyzed for two days against water, in order to eliminate the folic acid excess, and then concentrated using AMICON centrifugal device and quantified with the dried weight technique.

The functionalization rate of ORMOSIL-NH_3 with folic acid was established measuring the absorbance at 364 nm of 1 mg/mL solution of ORMOSIL-FA in NaOH 1M, and considering εFA_{364}= 9500 $M^{-1}cm^{-1}$.

Scanning Electron Microscopy study

Z-potential analysis of ORMOSILs

Z-potential measurements were carried out with a MALVERN Zetasizer apparatus equipped with a 5 mWHeNe laser. Low applied voltages were used to avoid the risk of effects due to Joule heating. The measurenets were done in collaboration with F. Bordi del dipartimento di fisica dell' Università La sapianza di Roma.

Athomic fource microscopy study of ORMOSILs(AFM)

The AFM measurements were performed using a home designed microscope in collaboration with M. Girasole from Istituto di Struttura della Materia - CNR, Rome, Italy, described in (Cricenti and Generosi, 1995) The isinstrument operate under controlled environmental conditions. The AFM measurements were performed in air, at room temperature and constant 30% relative humidity. The contact mode measurements were performed in the weak repulsive regime of constant force with a probe force below 1 nN from zero cantilever deflection.

ORMOSIL localization experiments

HeLa cell and H1299 were plated $1 \cdot 10^5$ cells in 24-well plate, 24 h before the treatement Cells were than treated with different amount of ORMOSIL-NH_3 or ORMOSIL-FA containing rhodamine β-isothiocianate for 2h in presence of RPMI(-)FCS with or without FA. The external medium was remover and cells cleaned tree times with PBS. Cells were than collected using 1mM EDTA solution in PBS, followed by a centrifugation 2.5 rpm 5´. Cells were than suspended in 1% w/v para-formaldehyde solution in PBS for 1h at 4 ºC. The fluorescence intensity was monitored by flow cytometry using FL1 channel for red fluorescence.

Synthesis of Chitosan /pDNA complex

The preparation of nanoparticles Chi/NP took place according to the Novamatrix protocol for the derivatives of ultra pure chitosan. Briefly, tow different mixes of equal final volume, were prepared containing respectively, plasmid DNA in nuclease-free water, and the specific chitosan in Na Acetate 30mM pH 5.5. The amount of the different pDNA mix is kept constant,

while chitosan is used in varying amounts depending on the N/P ratio of the producted nanoparticles.

(It is considered N/P = 1 for 1.32 µg pDNA and 0.48 µg Chi 100% DD). The 2 mixes were separately mixed whit vortex, then the mix containing pDNA was added to that with chitosan, and mixed with vortex continousely for 15" The final concentration of Na Acetate buffer was 15 mM. The Chi/pDNA nanoparticles were left 30' room temperature before using for caracterizarion or transfection experiments.

Synthesis of Lipofectamine®/pDNA complex

Lipofectamine® /pDNA complex were produced reacting 1µg of plasmid DNA with 5µL of Lipofectamine® reagent. Even in this case were prepered tow mixes of equal volum of DNA and Lipofectamine® reagent in RPMI without FCS. The mixes were gently mixed, then DNA mix was added to the other and left 30' room temperature before transfection experiments.

Particle side distribution and z-potential measurements

Has been measured through a zeta potential particle analyzer Zetasizer NANO-ZS and data analyzed with the

DTS(NANO) software. Particle formation have been monitored every time in 15mM Na Acetate buffer pH 5.5.

Transfection experiments

J774A-1 and H1299 cells were seeded $1 \cdot 10^5$ in 24-well plate 24h before transfection. Then cell medium was removed and cells washed with steril PBS.

250 µL of RPMI-mediun (-) FCS was replaced and cells were put in presence of Chi/pDNA complex with N/P=2.5, 5, 10 (reported in Novamatrix references to be the better N/P ratio for plasmide transfection (Köping-Höggård *et al*, 2003) or Lipofectamine®/pDNA complex with a final amount of GFP expressing plasmid DNA of 0.33µg for well.

After 4 h, medium was removed and cells washed 3 times with PBS and left grout for 44 h in the incubator in presence of RPMI with 10%FCS.

GFP production was observed by fluorescence microscopy.

Plasmid DNA and chitosan localization study

The localization studies were carried on in the same way of the transfection experiments, but nanoparticles were producted incubating, the Novamatrix ultra pure chitosan with a Cy3 labeled GFP-pDNA, or a Cy3 labeled chitosan 50 KDa almost 100%DD complexed with GFP-pDNA. Fluorescent nanoparticles were observed for the interaction with J774A-1 cells by fluorescence microscopy, after 4 h of transfection or the day later.

4. RESULTS

4.1 Results on MC-Chi-FA project.

Chitosan-folate complex formation and functionalization of microcapsules.

Chitosan-folate has been synthesized using published protocols (Wan *et al*, 2008) by reacting the NH2 group of chitosan with the COOH groups of folate (Figure 4.1-1).

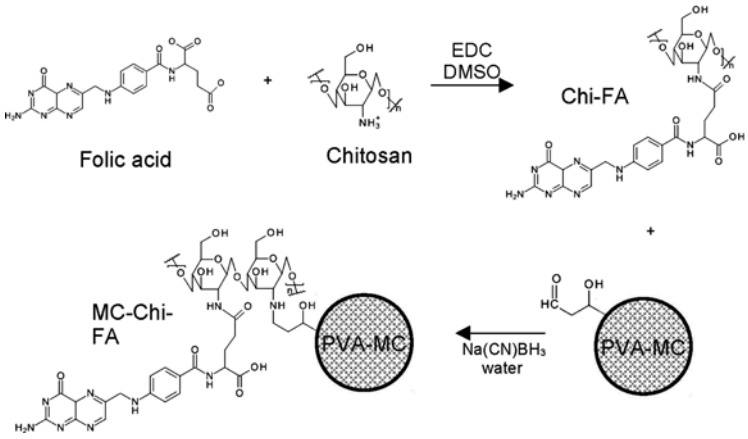

Fig 4.1-1: General scheme for the synthesis of chitosan-folate modified microcapsules (MC-Chi-FA). The chitosan-folate (Chi-FA) derivative is obtained by reacting chitosan and folate in DMSO using EDC to activate the COOH folate groups. Chi-FA is linked to MC using a reductive amination procedure.

The γ-carboxylate group is the most reactive one, although the α-carboxylate is also available for conjugation. The reaction has been verified through ^{1}H NMR spectroscopy that is not able to distinguish between the two contributions. The 1H NMR spectrum of chitosan (Figure 4.1-2a) shows a series of peaks corresponding to protons linked to the C3, C4, and C2 carbon atoms of the sugar and to the methyl protons, falling at 3.90, 3.77, 3.18, and 2.07 ppm, respectively. The degree of chitosan deacetylation, obtained from the ratio of the integrals of the methyl peak over the C2 one, is found to be 85%. The 1H-NMR proton spectrum of chitosan-folate (Figure 4.1-2b), when compared to chitosan, shows additional peaks at 8.73, 7.66, and 6.83 ppm, due to the folate aromatic rings and one at 2.40 ppm, due to the protons linked to C22 (see insert of Figure 4.1-2 for the labeling of the different groups). The ratio between the integral of one of the folate aromatic peaks and the chitosan C2 peak at 3.14 ppm allows us to quantify the percentage of folate substitution on the chitosan NH2 groups, that is found to be 5%. On the basis of nominal molecular weight, this

percentage corresponds to 15 folates per chitosan molecules.

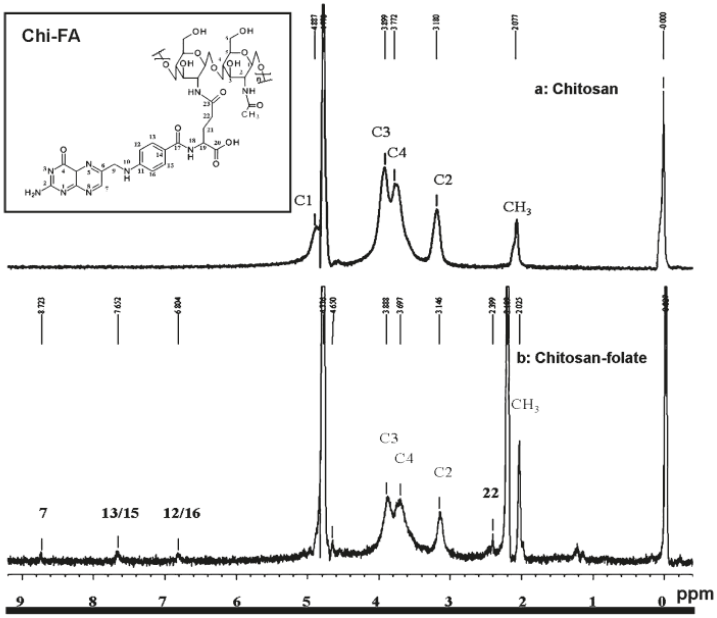

Fig 4.1-2: NMR spectra of chitosan and of the chitosan-folate derivative. (a) 1H-NMR spectrum of chitosan solution in D2O with 3% (v/v) CD3COOD; (b) 1H-NMR spectrum of 3 mg/mL of the chitosan-folate adduct in D2O with 3% (v/v) CD3COOD. Inset: Chemical structure of the chitosan_folate complex. In gray, the numbering of carbons of chitosan; and in black, the numbering of folate (see text for peak assignments).

Chitosan and chitosan-folate have been also functionalized with rhodamine (Rod) to give the Chi-Rod and Chi-FA-Rod complex.

All the synthesized complexes have been then conjugated to microcapsules (MC) using the reductive amination procedure in the presence of $Na(CN)BH_3$ (Cavalieri *et al*, 2006) (Cavalieri *et al*, 2005), to yield MC-Chi, MC-Chi-FA or MC-Chi-Rod, MC-Chi-FA-Rod. The success of decoration is verified by using the rhodaminated derivatives of chitosans (Figure 4.1-3).

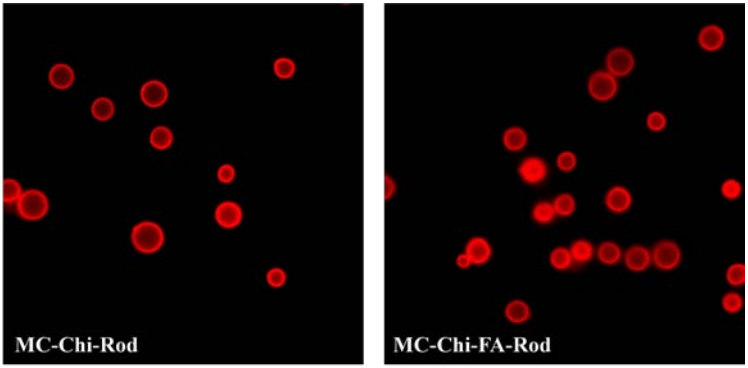

Fig 4.1-3:. Fluorescence microscopy of decorated MC. Left panel shows the rhodamine signal of Chi-Rod on MC, the right one the rhodamine signal of Chi-FA-Rod on MC surfaces, indicating the successful functionalizations.

Size distribution and Z-potential measurements.

Differently coated microcapsules in solution have been characterized in size and Z-potential by dynamic light scattering (DLS). On the basis of the size distributions shown in Figure 4.1-4, MC, MC-Chi and MC-Chi-FA have average diameters values of 3.1 ± 0.3, 4.2 ± 0.1 and 3.0 ± 0.1 μm, respectively.

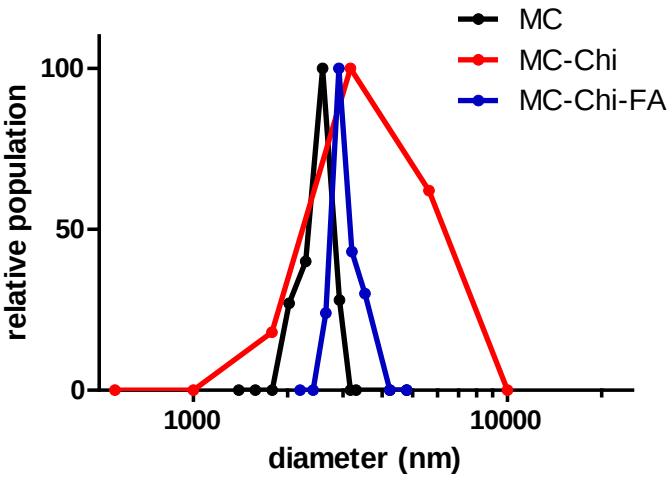

Fig 4.1-4: Average hydrodynamic diameters for MC (black line), MC-Chi (red) and MC-Chi-FA (blue) in water solution.

The size distribution of MC-Chi includes larger diameters than the distributions of MC and MC-Chi-FA, indicating a large tendency to aggregate. Table 4.1-1 shows the Z-potential vales for the different type of structures.

Sample	Dh (µm)	Z potential (mV)
MC	3.1±0.3	-7
MC-Chi	4.2±0.1	+8
MC-Chi-FA	3.0±0.1	-18

Tab 4.1-1: Hydrodynamic diameters and zeta potentials of MC with different coatings.

Uncoated microcapsules are characterized by negative values of Z-potential, probably ascribed to the presence on the shell of some carboxyl groups, due to the over oxidation of some aldehyde functionalities during the splitting reaction with periodate or due to the oxidation by the oxygen dissolved in the dispersion medium. MC-Chi exhibits a slightly positive Z-value due to the coating with the positive chitosan molecules. MC-Chi-FA have a

more negative Z-potential than nude MC, as result of the introduction of the folate on the microcapsules shells. This surface potential stabilizes the colloidal dispersion of Chi-FA coated microcapsules contributing to depress the aggregation tendency of microcapsules coated with chitosan, as evidenced by the size distribution result on MC-Chi.

Camptothecin adsorption on the different MC's derivatives.

CPT shows an intrinsic fluorescence due to the aromatic moieties present in its scaffold, with a maximum absorbance at 370 nm (Kang *et al*, 2002), that can be useful to assess the loading of CPT on the functionalized microcapsules surface. Fluorescence microscopy images of MC-Chi and MC-Chi-FA equilibrated in a loading solution containing CPT at a concentration of 100 μM, after elimination of unspecifically adsorbed drug molecules are shown in Figure 4.1-5. The presence of CPT and of rhodamine labelled Chi-FA coating was monitored separately recording the fluorescence signal of the blue and red fluorescence channels of the microscope.

This is possible because of the well separated emission fluorescence of CPT (λex = 370 nm, λem = 420 nm) and rhodamine (λex = 540 nm, λem = 600 nm) in water (Dey and Warner, 1997) (Nabiev *et al*, 1998). The overall fluorescence indicates that CPT is efficiently loaded on rhodamine-labelled MC-Chi and MC-Chi-FA.

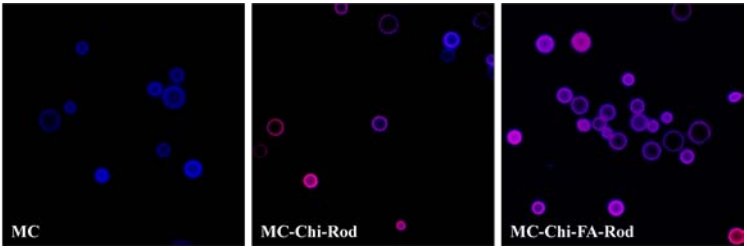

Fig 4.1-5: Fluorescence microscopy images of MC (left), MC-Chi-Rod (center) and MC-Chi-FA-Rod (right) adsorbed with CPT (blue signal). The blue signal is present in all the samples, while the red signal is due to the functionalization with Chi-Rod and Chi-FA-Rod, and is not present in nude MC

Figure 4.1-6 shows the binding isotherms of CPT by MC, MC-Chi and MC-Chi-FA equilibrated in an aqueous solution with different amount of CPT. In uncoated MCs the loading capacity at saturation is 50 % (w/w) of the

CPT in the loading solution, whereas MC-Chi and MC-Chi-FA show a high loading efficiency of about 85 % of the external drug in saturating conditions.

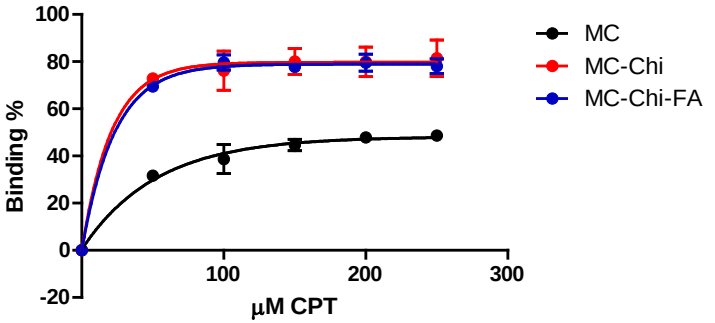

Fig 4.1-6: Binding isotherms of CPT on MC, MC-Chi and MC-Chi-FA surfaces in water

The release of the loaded CPT has been determined monitoring the amount of drug in the external medium, replaced every three days to remove the released CPT. The cumulative amount of released CPT in water, as a function of the concentration of CPT present in the loading solution is reported in Figure 4.1-7.

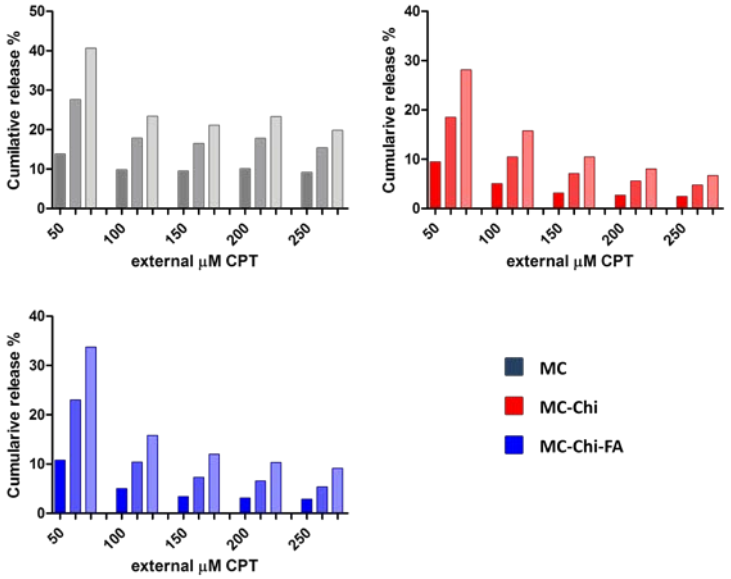

Fig 4.1-7: Cumulative release of CPT from the different microcapsules in water at 37 °C. The lightering of colors in the histograms represent the change of the external medium made every three days

Comparison in the release behavior between uncoated MC and MC-Chi and MC-Chi-FA indicates that CPT is detached from the uncoated system in larger extent for all the investigated loading conditions. MCs adsorbed with a large amount of drug, release percentually less than MCs adsorbed with low CPT concentration for all

functionalizations tested. Consistently with the loading data in Figure 4.1-6, these findings confirm a higher affinity of the coated MCs for CPT. To further address this issue, we have carried out release tests in the presence of phosphate buffered saline solution at pH 7.4 (Figure 4.1-8).

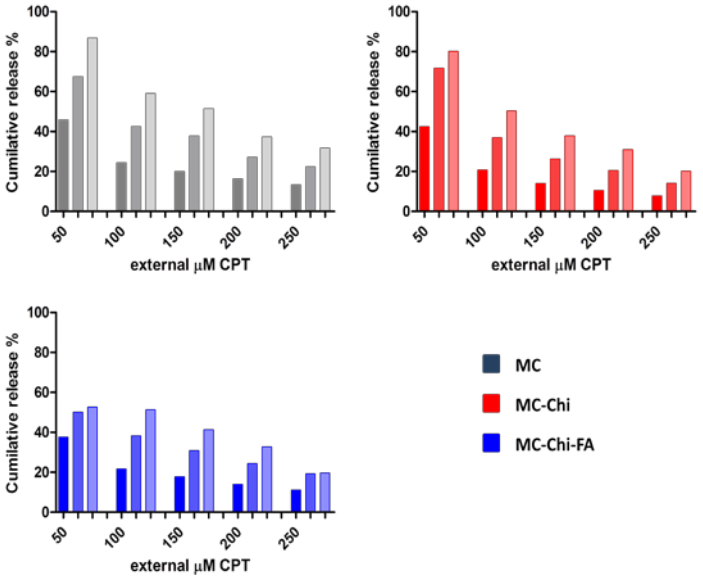

Fig 4.1-8: Cumulative release of CPT from the different microcapsules in PBS at 37°C. The lightering of colors in the histograms represent the change of the external medium made every three days

As expected, there are differences in the release behavior in presence of salt. Uncoated microcapsules increase their release around 2.2 fold, whereas the most marked difference occurs in the release of CPT from MC-Chi and MC-Chi-FA, where the stabilization of the drug cargo is remarkably attenuated likely because of the charge screening effect of the buffer. Functionalized microcapsules release in phosphate buffer around 4 times the amount of drug that normally is released in water. A possible explanation is that the presences of salt destabilize some interaction between CPT and chitosan coating. From this point of view also the enhancement of the loading capacity for MC-Chi and MC-Chi-FA can be the result of a favorable interaction (for exemple hydrogen bond) between the lactone form of CPT and the chitosan surface matrix (Figure 10).

A time release curve has been obtained for the different microstructures adsorbed with 100 μM of CPT. The release is monitored as a function of time by measuring the absorbance, A, of the CPT released by the

microcapsules in different type of media. In Figure 4.1-9 the one obtained in PBS at 37°C is reported.

The curve has been fitted with a single exponential function, indicating that the detachment of the drug from the Chi-FA coated vector is a first order diffusion process.

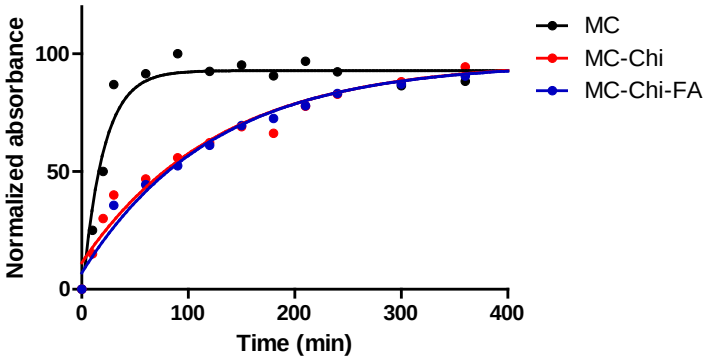

Fig 4.1-9: Drug release kinetics from MC (black), MC-Chi (red) and MC-Chi-FA (blue) in phosphate buffer pH 7.4 at 37°C. The analysis shown different K value respectively K_{MC} = 0.024±0.027, $K_{MC\text{-}Chi}$ = 0.0081±0.0013 and $K_{MC\text{-}Chi\text{-}FA}$ = 0.0072±0.00088.

A single exponential fitting curve, A = Amax[1 - exp(Kt)], suitably describes the time dependence of the process indicating a first order release with a

characteristic release time, K^{-1}, three fold larger in the case of the coated microcapsules with respect to the uncoated ones. This result means that the coating has an active role in the loading as well as in the release phase.

The release kinetics has been monitored also in presence of D-MEM (Figure 4.1-10a) and D-MEM supplemented with 10% serum at 37°C (Figure 4.1-10b)

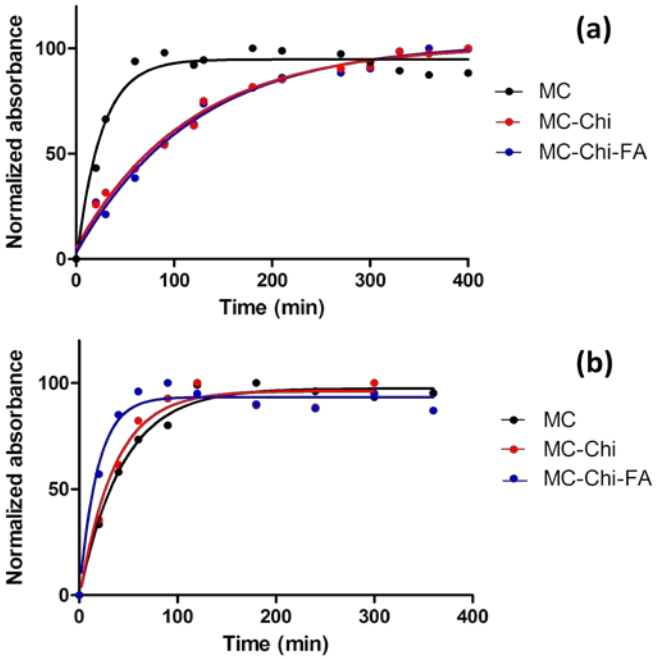

Fig 4.1-10: Serum effects on CPT release kinetics. Normalized release of CPT from microcapsules in D-MEM (a) and D-MEM with 10% of FCS (b) at 37 °C.

In presence of culture medium (Figure 4.1-10a) the release kinetics doesn't change so much with respect to the release kinetics in PBS. The K^{-1} values in D-MEM at 37°C, derived from the fit are: K_{MC} = 0.040±0.005, K_{MC-Chi} = 0.0086±0.0008 and $K_{MC-Chi-FA}$ = 0.0083±0.0009. Also in these conditions it is observed that functionalized MC are 2 fold slower in the release of CPT than the nude one.

The release profile from the structures dramatically change in presence of 10% FCS (Figure 4.1-10b), that cause an increase of the release speed for all the structure tested; the K value of the curves become K_{MC} = 0.023±0.002, K_{MC-Chi} = 0.0028±0.004 and $K_{MC-Chi-FA}$ = 0.0054±0.008, respectively.

Interaction of MC with different cell lines.

The ability of MC and MC-Chi-FA to interact with cells has been tested incubating the capsules with two different cell types: HeLa cells, that overexpress the FR, and NIH3t3 fibroblasts, not expressing the receptor on their

surface, as a negative control. The cells have been incubated for two days with 100 μg/mL of MC, MC-Chi, and MC-Chi-FA, all labeled with rhodamine-β-isothiocyanate on PVA, and then they have been extensively washed, stained, and imaged. Representative images from these experiments are shown in Figure 4.1-11.

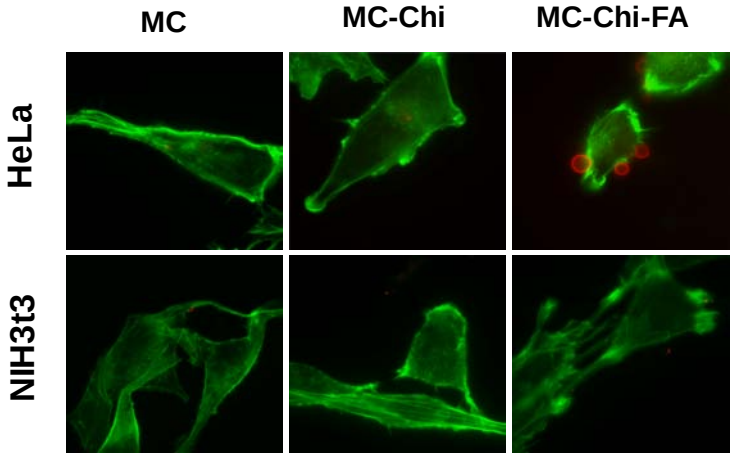

Fig 4.1-11: Localization of MC on the cells. Fluorescence microscopy image of HeLa tumor cells (up) and NIH3t3 fibroblast cells (down), treated for 48 h with MC (left), MC-Chi (middle), and MC-Chi-FA (right). The cells have been cultured in folate-free conditions.

Control cells show no uptake of MC, independent of their functionalization, while HeLa cells exhibit a folate-dependent interaction. In our experiments, the unfunctionalized MC have never been found to interact with HeLa cells, while a small number of adhesions has been occasionally found for MC-Chi, likely due to a fusogenic activity of chitosan. In marked contrast, MC-Chi-FA frequently interact with the surface of HeLa cells as shown in Figure 4.1-12 where a large number of folate modified microcapsules is bound to cancer cells.

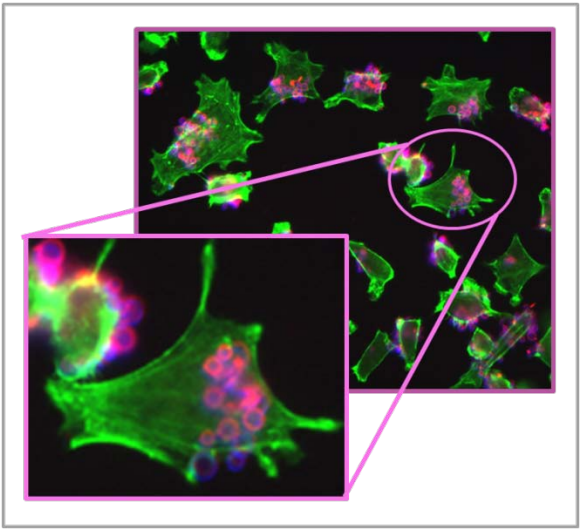

Fig 4.1-12: Hela tumor cells (green signal) interacting with MC-Chi-FA in folate free media, MC-Chi-FA were rhodaminated on PVA shell (red signal) and adsorbed with CPT 100µM (blue signal)

The internalization of MC Chi-FA by HeLa cells can be appreciated through a series of optical sections above and below the focal plane of the cell, such as the ones reported in Figure 4.1-13, where a representative sequence from outside to inside the cell is shown.

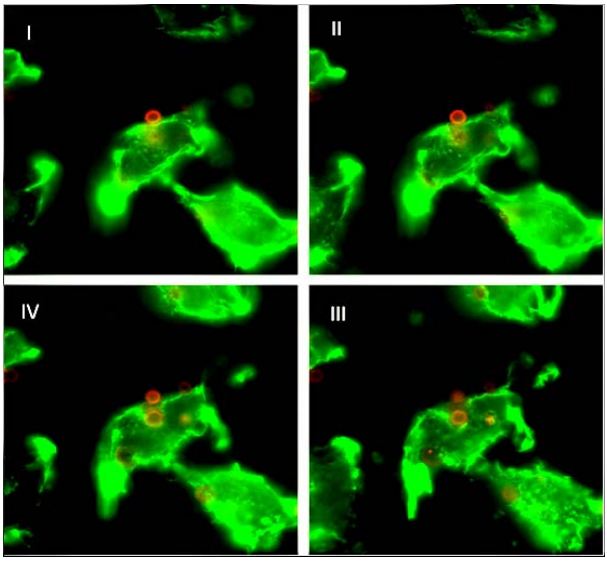

Fig 4.1-13: Optical sections above and below the focal plane of the HeLa cell (green signal) interacting with the MC-Chi-FA (red signal). The number I-IV indicates sections from the outside to the inside of the cell, and presents the race in number of microstructures that become visible in to the cell.

A further hint to the nature of folate-mediated interaction is given by competition experiments, in which functionalized MC have been administered to cells in presence of free folate in the medium. The effect of competition is striking, since in this case the uptake of MC-Chi-FA is substantially suppressed (Figure 4.1-14).

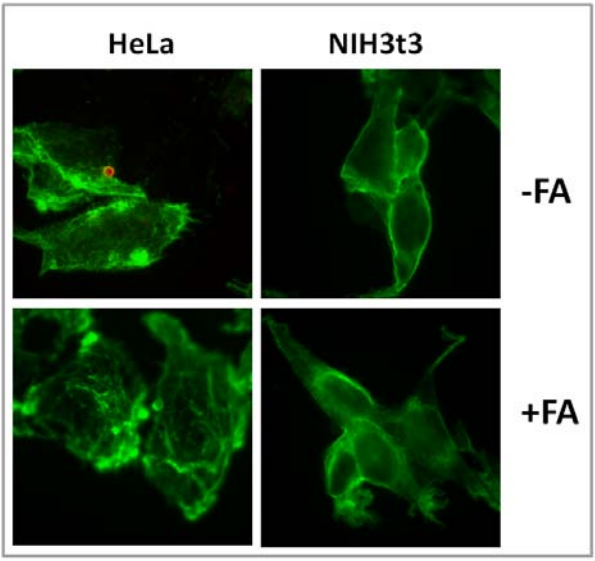

Fig 4.1-14: Localization of MC-Chi-FA (red) on HeLa cell and HIH3t3 control cell 8green) in presence or absence of free folic acid in the medium

The impact of MCs on healthy and cancer cells has been followed, incubating cells in the presence of MC, MC-Chi, and MC-Chi-FA, either previously adsorbed with CPT or not. For drug adsorption, the microcapsules have been incubated with 100 μM CPT, and the amount of drug adsorbed was quantified. The quantity of MC used for the cell treatment is different and depends on the MC functionalization. For each experiment, we have taken care to have a concentration of adsorbed CPT equal to the IC_{50} of the specific cell line. In detail, a CPT concentration of 40 nM, corresponding to the IC_{50} value for the HeLa cells (Takara *et al*, 2009), and one of 12 μM, corresponding to the IC_{50} for the NIH3t3 (Suzuki *et al*, 2003) have been used. The cells have been incubated with the microcapsules for 48 h and allowed to grow on fresh medium for additional 48 h before being assayed on their proliferation (Figure 4.1-15). This method has been established to allow the discrimination of the effect due to the diffusion of the drug lost from the capsules in the medium from the one due to a direct capsules-cell interaction.

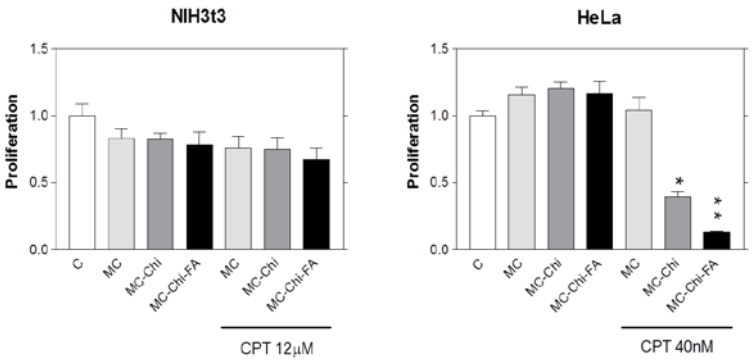

Fig 4.1-15: Effect of the decorated MC on cell lines. Proliferation of NIH3t3 fibroblast (left) and HeLa cells (right), treated for 48 h with MC, MC-Chi, and MC-Chi-FA, with or without CPT adsorption. The treatment was removed and substituted with fresh medium, and then the proliferation was assayed after 48 h. Asterisks mark statistical significance ($p < 0.01$).

In the absence of CPT, a difference in proliferation no larger than 10% has been found on both cell lines for any kind of incubated MC. In presence of adsorbed CPT, the anti-proliferative effect of the microcapsules is slightly larger in the HeLa than in the control NIH3t3 cells for the MC-Chi system, a phenomenon that is not easy to interpret, although a more intense interaction of chitosan with HeLa cells could account for it. The most striking difference is observed upon incubation with the MC-Chi-

FA. In this latter case, in fact less than 20% cells survive in the case of HeLa cells, while more than 80% of NIH3t3 cells are still active. This result confirms that the over expression of the folate receptor permits a very efficient and selective targeting of HeLa cells by the MC-Chi-FA.

4.2 Results on MC-Lys-FA project

Functionalization of MC with Lysine and Folic acid

PVA microcapsules has been functionalized with lysine by exploiting the presence of aldehyde groups on the shell's surface of the structure that can react with one of the two aminic groups of the aminoacid lysine The other aminic group has been used to link folic acid via a coupling reaction as shown in Figure 4.2-1.

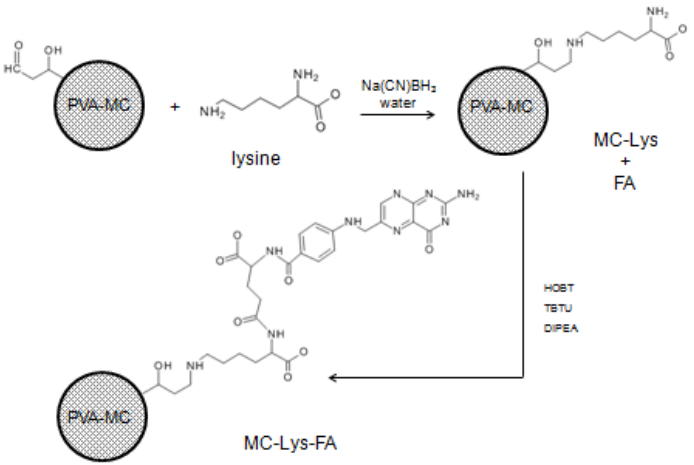

Fig 4.2-1: Schematic representation of the two steps chemical procedure to produce MC-Lys-FA. The first step is the linkage of lysine, that is then used for folic acid conjugation.

The first reaction between lysine and PVA is not specific, and there is no way to distinguish the direction of the lysine's arm between PVA and folic acid. It's called reductive amination procedure and leads to the formation of a Schiff base, that is then reduced and stabilized by sodium cyano-borohydride.

The second reaction, the linkage of folate, is catalyzed by coupling reagents that increase the reactivity of the carboxylic groups of the folic acid, transforming them into an activated ester, able to interact with the amine group of lysine generating an amide bond (Figure 4.2-1). The amount of folic acid conjugated is quantified measuring the absorbance of MC-Lys-FA dissolved in 1M NaOH, subtracting the absorbance of a MC-Lys solution at identical concentration (Figure 4.2-2).

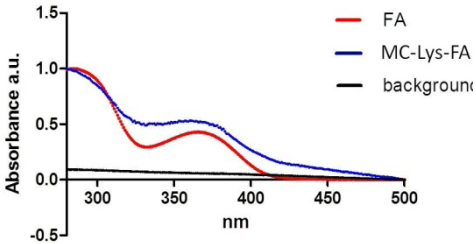

Fig 4.2-2: Comparison of the absorption spectra of folic acid with MC-Lys-FA. the background represent the absorption of MC-Lys. All the spectra were acquired in 1M NaOH.

The typical folic acid concentration on MC-Lys-FA is $4.8 \pm 0.025 \cdot 10^{-9}$moles FA / mg of microstructure.

Size distribution and Z-potential measurement

The MC, MC-Lys and MC-Lys-FA structures have been analyzed in dimension and Z-potential. Figure 4.2-3 shows the size distributions measured in water using DLS. All the structures have an hydrodynamic diameter ranging between 2µm and 4µm, in particular d_{MC} = 3.2±0.5µm, $d_{MC\text{-}Lys}$ = 2.6±0.7 µm and $d_{MC\text{-}Lys\text{-}FA}$ = 2.7±0.4. The microcapsules show an average size slightly larger than the functionalized ones, suggesting that the functionalization with lysine gives rise to electrostatic repulsion, ensuring a large dispersion in water.

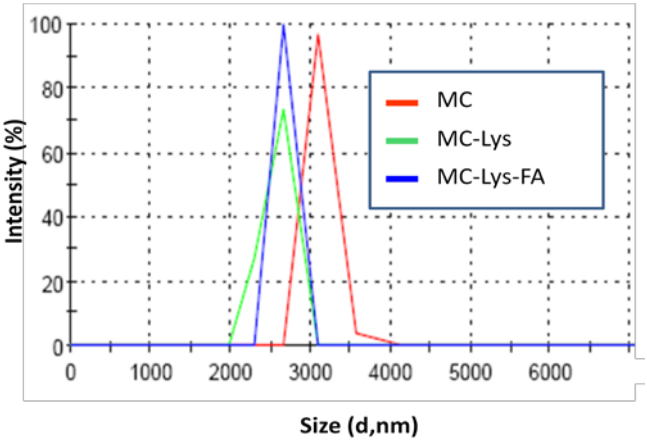

Fig 4.2-3: Size distribution of microcapsules in each population.

Figure 4.2-4 reports the Z-potential distribution obtained in water.

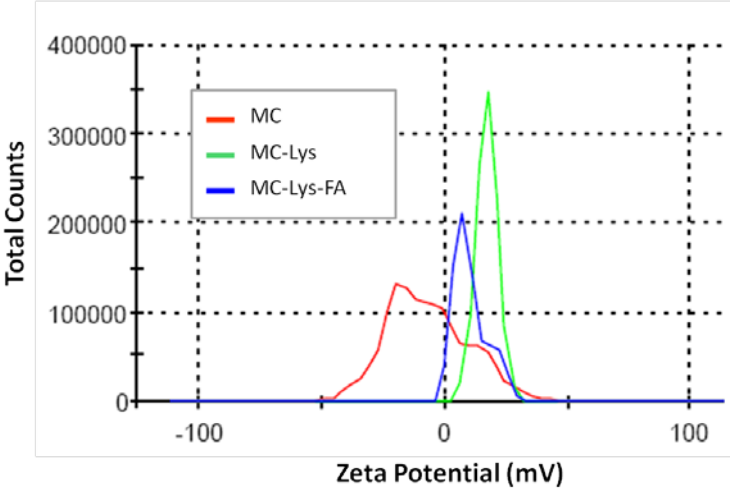

Fig 4.2-4: Z-potential distribution of each population of microcapsules, the functionalization is increase the zeta potential due to the presence of positively charged groups, particularly in the microcapsules decorated with lysine alone.

The results indicate that the average surface potentials are -6.4, 17.6 and 10.8 mV for MC, MC-Lys and MC-Lys-FA respectively, with a polydisperse distribution for MC. The Z-value for MC-Lys is significantly increased respect to the one of nude MC, confirming the succesfull of the first functionalization step, while MC-Lys-FA show an intermediate surface potential indicating that

some of the positive amino groups of lysine have been covered by the folate.

Characterization of adsorption and release of camptothecin from PVA-MC, MC-Lys and MC-Lys-FA

The drug binding and release from PVA microcapsules have been assessed following the absorption at λ=370 nm corresponding to the maximum of CPT. After four days of incubation with 100μM camptothecin in water, the loading capacity of nude microcapsules represents the 51.2% of the external drug concentration (in agreement with previous data), whilst for microcapsules functionalized with lysine and folic acid the values are 95.5% and 95.9% respectively (Figure 4.2-6). The release kinetics has been measured resuspending the capsules adsorbed with CPT in culture medium (RPMI1640, (-) phenol red,) supplemented with glutamine (1%), antibiotics (1%) and heat inactivated serum (10%), at 37°C (Table 4.2-1). The rate of CPT released from MC-Lys and MC-Lys-FA is 10 times and 5 times slower

respectively than for nude MC, also in presence of serum that causes an increase in the rate (see Figure 4.1-10a/b). The data for the absorption and release experiments are summarized in Table 4.2-1.

Sample	% Abs	% Rel	K-value	Half-life (min)
MC	51.2	10.1	0.22±0.071	3.12
MC-Lys	95.5	25.3	0.018±0.0028	39.2
MC-Lys-FA	95.9	17.9	0.037±0.0034	18.6

Tab 4.2-1: Summery table for the experiment of absorption and release of CPT with the microstructures. The release percentages are referred to the total amount of CPT adsorbed on the MCs surface. The k-value and half life reported in table are obtained in complete cell culture medium.

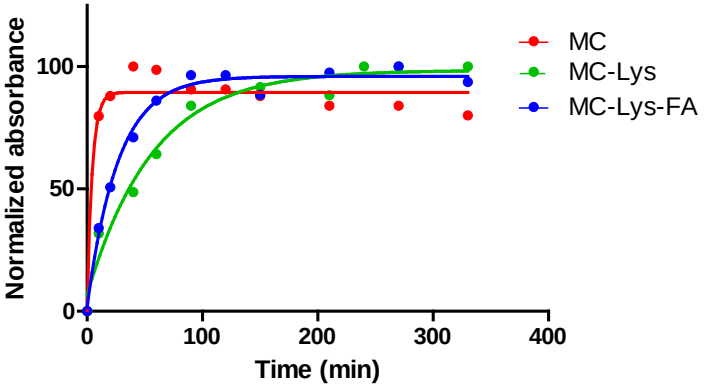

Fig 4.2-5: Release profile of nude and functionalized microcapsules, analyzed with a single exponential fitting curve, A = Amax[1 - exp(Kt)]. The K-value obtained are respectively K_{MC} = 0.22±0.07, $K_{MC\text{-}Lys}$ = 0.018±0.003 and $K_{MC\text{-}Lys\text{-}FA}$ = 0.037±0.003.

Immuno-fluorescence study of the folic acid receptor expression

The differential expression of folate receptor (FR) in tumor cells lines of epithelial origin (HeLa and H1299) and in control healty cells of connective origin (NIH3t3 fibroblast) have been assayed by immune-fluorescence (Figure 4.2-6).

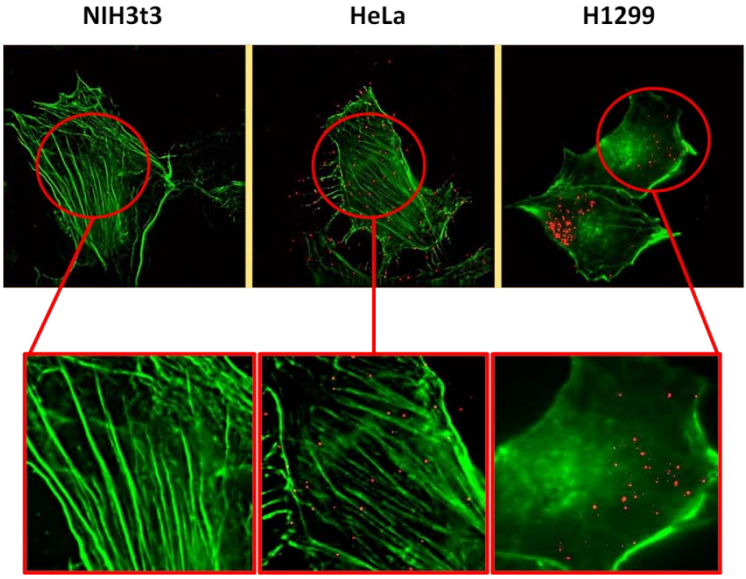

Fig 4.2-6: Immune-fluorescence for the folate receptor (FR) on the three cell lines on which the structures were tested. The lower panels are magnifications of the upper panel. The receptor is expressed in tumor cell lines (HeLa and H1299), while is not expressed in control cells (NIH3t3).

The experiments have been done without permeabilizing the cell membrane, in order to visualize only the membrane associated pool. A primary antibody against human FR and a secondary antibody, labeled with Alexafluor 555 (red fluorescence), have been used in the experiment. The red signal, diagnostic of the FR presence, is observed only in HeLa and H1299 cells but the interpretation of the signals distribution is not straightforward since the FR accumulation into discrete clusters is dependent on cross-linking reaction by secondary antibody (Anderson, 1993; Anderson *et al*, 1992; Mayor *et al*, 1994), Nevertheless, the immune-fluorescence assay shows an expression of FR in tumoral cells significantly larger than in fibroblast control cells, that do not have detectable levels of folate receptor.

The result is also confirmed by flow cytometer analysis (FACS-analysis) showed in Figure 4.2-7 as normalized red fluorescence (normalized geometrical mean), corresponding to the differential FR expression in the cell lines.

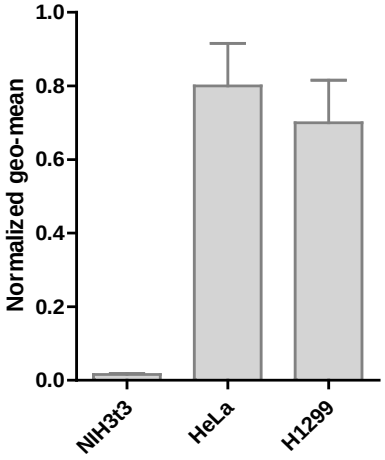

Fig 4.2-7: FACS analysis of the different cell lines labeled with secondary antibodies conjugated with Alexafluor 555. Normalized average geometrical mean of the FL1 channel (red fluorescence) The data were subtracted from the cell line specific auto-fluorescence value, and from the non specific secondary antibody background.

Interaction of MC, MC-Lys and MC-Lys-FA with different cell lines.

The ability of MC and MC-Lys-FA to interact with cells has been tested, incubating the capsules with the three different cell lines. The cells have been incubated for 24h with 100 μg/mL MC, MC-Lys or MC-Lys-FA in normal RPMI or folate free-RPMI medium, in order to observe the competition between the free folic acid and the folic acid linked on the microcapsules surface. All MCs have been labeled with rhodamine-β-isothiocyanate on PVA

shell, while the cell cytoskeleton have been labeled with phalloidine-FITC. Representative images concerning the localization experiments for HeLa cells are shown in Figure 4.2-8,

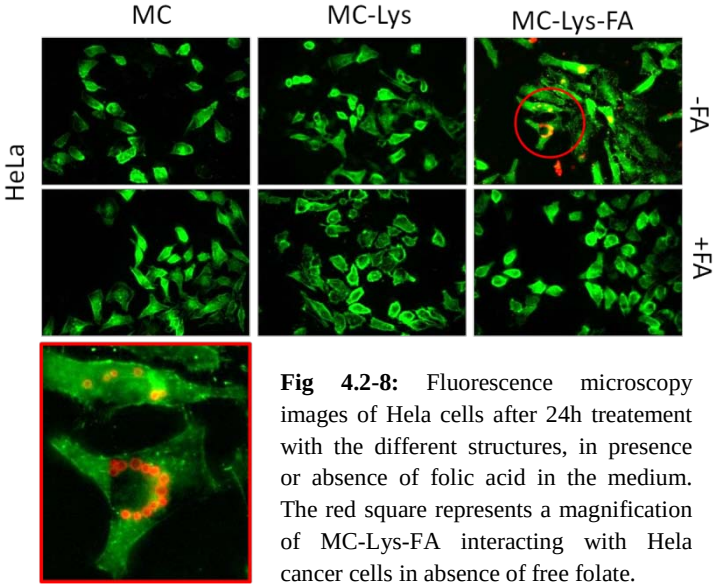

Fig 4.2-8: Fluorescence microscopy images of Hela cells after 24h treatement with the different structures, in presence or absence of folic acid in the medium. The red square represents a magnification of MC-Lys-FA interacting with Hela cancer cells in absence of free folate.

The images indicate that HeLa cells do not interact with MC and MC-Lys in all the experimental conditions, while MC-Lys-FA do interact with HeLa cell. On the other hand HeLa and MC-Lys-FA in presence of folic

acid do not show any interaction, indicating that free folic acid competes for the binding to the folate receptor and that the interaction between MC-Lys-FA and Hela cells is receptor-mediated. A similar result has been found for the H1299 tumor cell line shown in Figure 4.2-9.

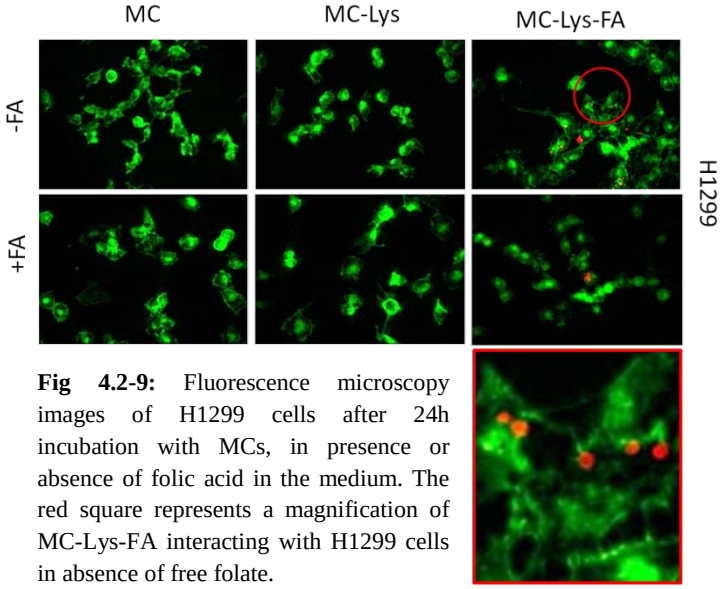

Fig 4.2-9: Fluorescence microscopy images of H1299 cells after 24h incubation with MCs, in presence or absence of folic acid in the medium. The red square represents a magnification of MC-Lys-FA interacting with H1299 cells in absence of free folate.

MC and MC-Lys are not able to interact with H1299 cells, independently of the presence or absence of folic

acid in the culture medium. MC-Lys-FA interact with the cells in absence of external folate and the interaction is strongly affected by the presence of FA.

NiH3t3 control cells are never able to interact with MCs, confirming that MC-Lys-FA discriminate between cell lines having or not the folic acid receptor (Figure 4.2-10).

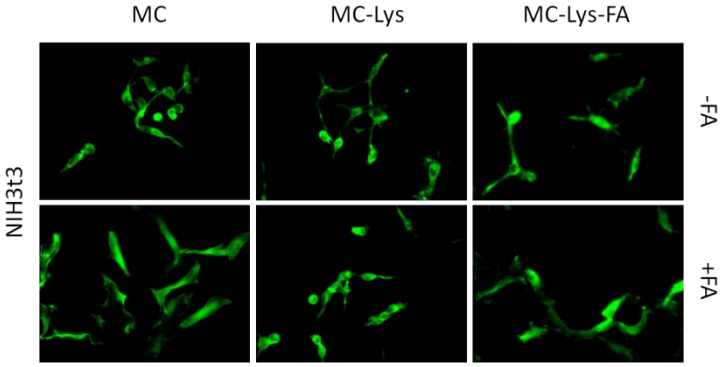

Fig 4.2-10: Fluorescence microscopy images of NIH3t3 control cells after 24h treatement with the different structures, in presence or absence of folic acid in the medium.

The number of microcapsules/cells has been quantified for HeLa and H1299 cells. The analysis have been done for 5 slides of each treatment for 3 independent

experiments for a total of 400 cells for each treatment. The results indicate an average of 1.5±0.6 MC-Lys-FA/n° cell for HeLa cells and 0.7±0.25 MC-Lys-FA/n° cells for H1299 cells.

Cells viability experiments

The IC_{50} value of the different cell lines for CPT has been calculated after 24h of treatment, the same time interval used to study the MC-Lys-FA/cells interaction. It is necessary to consider the differential toxicity of CPT in the cell lines in order to appropriately set the proliferation experiment conditions of the CPT loaded MCs. An IC_{50} value of 13µM, 40 µM and 12 µM has been found for HeLa, H1299 and NIH3t3 cells respectively (Figure 4.2-11).

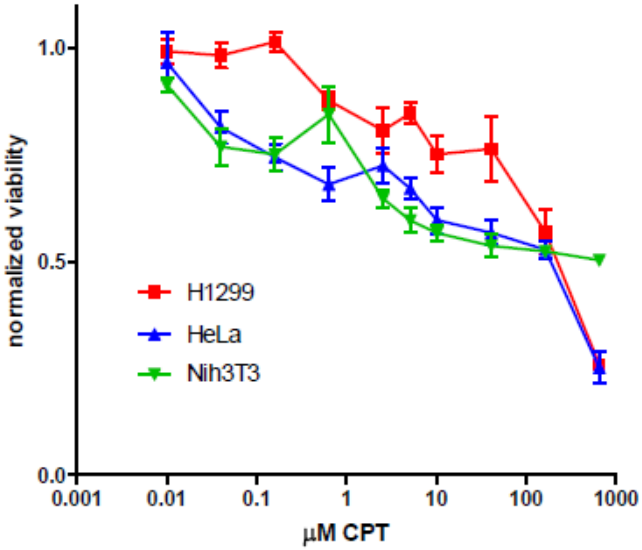

Fig 4.2-11: IC_{50} curves obtained using different CPT concentration in culture medium. Cell viability is calculated after 24h of treatment

4.3 Results on Silica Oil/Water microemulsion project.

Oil in water micro-emulsions have been produced according to literature (Qian *et al*, 2008) and functionalized with folic acid in order to selectively recognize tumor cells of epithelial origin. In Figure 4.3-1 the chemical synthesis used for the direct linkage of folic acid to ORMOSIL nanoparticles is shown.

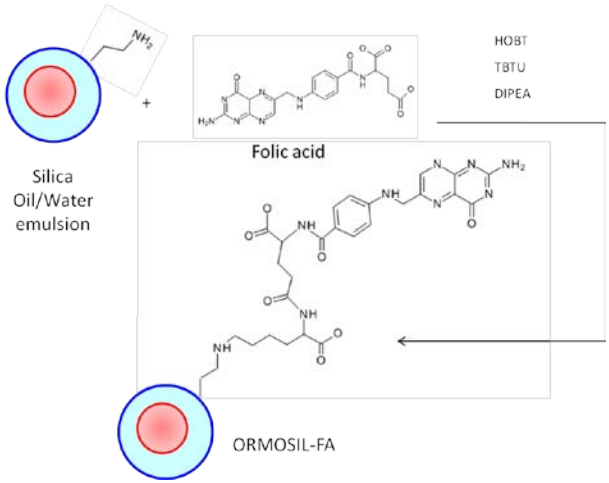

Fig 4.3-1: Schematic representation of the chemical synthesis of the ORMOSIL-FA with a direct linkage of folic acid

The reaction is catalyzed by coupling reagents to produce an activated ester on the carboxylic folic acid groups that react with the NH_3 groups of the APTES layer of the oil in water microemulsion, giving rise to ORMOSIL-FA nanoparticles containing $3.75 \pm 0.35 \cdot 10^{-8}$ mol FA/mg ORMOSIL-FA.

Characterization of oil in water emulsion (ORMOSIL-NH_2) and the folic acid derivative (ORMOSIL-FA)

The oil in water microemulsion has been characterized by scanning electron microscopy (SEM) and atomic force microscopy (AFM). Figure 4.3-2 shows the SEM images of the samples dried on a silica wafer support and covered with gold, in order to have a conductive material able to generate a signal. The images show particles with a relatively uniform spherical shape and diameter ranging between 30 and 40 nm. The reaction with folic acid does not alter the morphology of the structures.

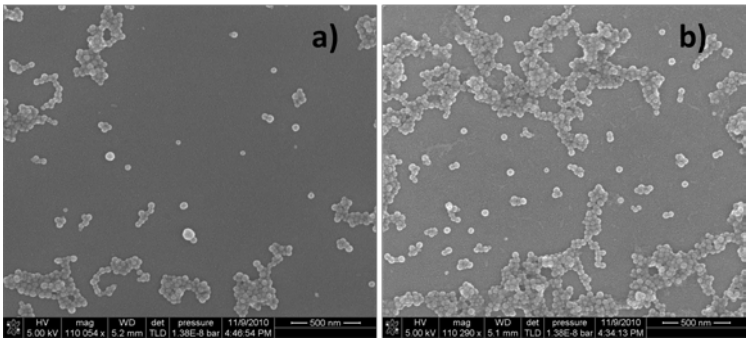

Fig 4.3-2: Scanning electron microscopy images of a) ORMOSIL-NH_3 and b) ORMOSIL-FA dried on silica wafer and covered with gold. Referring to the scale bar the nanoparticles have aa average diameter of 35 nm

In Figure 4.3-3 the AFM images for ORMOSIL-FA are shown at two levels of magnification. In the left panel the scanning area is 8x8 µm, while in the right panel is 3x3 µm. The particles have a diameter around 60 nm. The discrepancies between the DLS and AFM data can be attributed to the tip convolution effects of the atomic force microscopy.

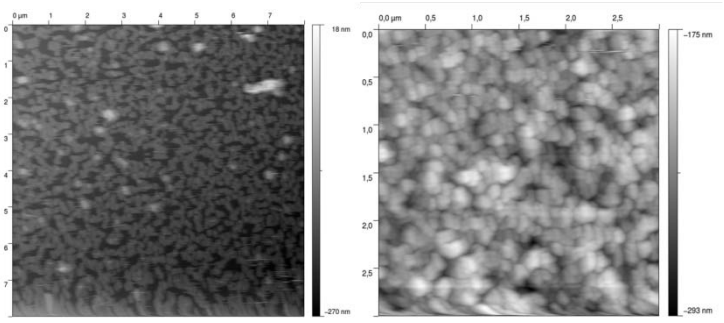

Fig 4.3-3: Atomic force microscopy images of ORMOSIL-FA in gray scale ranging between -270 to 18 nm (left panel) and -293 to -175 (right panel).

The DLS particles distribution and Z-potential results are reported in the Table 4.3-1.

Sample	d(nm)	Z-potential (mV)
ORMOSIL-NH2	70.3±2.3	-9.9
ORMOSIL-FA	69.2±2.1	-14.6

Tab 4.3-1: Particle diameter and Z-potential measurements

The DLS measurements indicate a hydrodynamic diameter of around 70 nm, close to the value obtained from AFM. The chemical modification with folic acid

does not change the particle dimension, demonstrating that the particles are well dispersed in the solution. The surface charge of the amino functionalized particles is negative (-9.9 mV), probably due to the high content of VTES in respect to APTES during the nano-emulsion production. It becomes even more negative (-14.6) when the amine of APTES is covered with folic acid, due to the amine neutralization and/or to the presence of the free carboxylic groups of the folic acid.

Cell culture experiments

The ability of ORMOSIL-NH_2 and ORMOSIL-FA to accumulate in cells has been tested by flow cytometry, measuring the normalized red fluorescence intensity of HeLa and H1299 cells after 2h of treatment, in folic acid and serum free medium, with ORMOSILs containing rhodamine β-isothiocianate in the internal core. The results in figure 4.3-4 indicate that ORMOSIL-NH_2 uptake is more efficient than the one of the ORMOSIL-FA, likely because of its less negative Z-potential value.

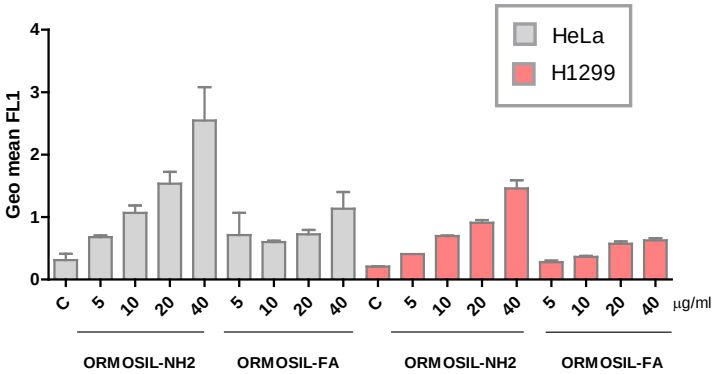

Fig 4.3-4: Particles uptake by HeLa and H1299 cells after 2h treatment in RPMI folate and serum free. FACS analysis that show the geometrical mean of the FL1 channel in respect to particles concentration.

The uptake of ORMOSIL-FA by H1299 in folic acid free condition is saturable at around 20-40µg/ml.

Competition experiments between ORMOSIL-FA and free folate, done for HeLa and H1299 cells changing the ORMOSIL-FA concentration (Figure 4.3-5) confirm that the particles uptake is a saturable process.

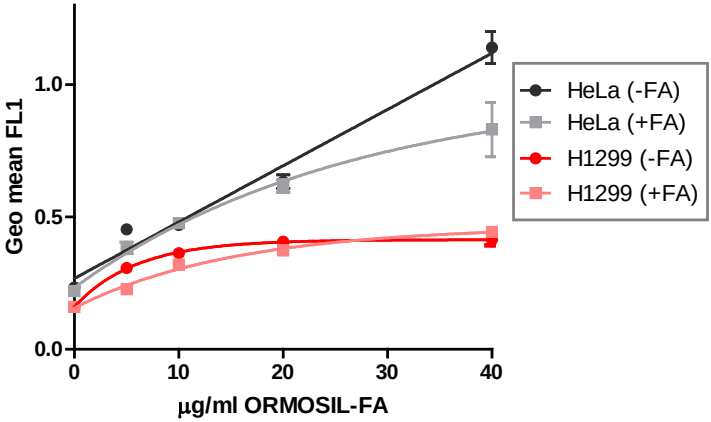

Fig 4.3-5: Dose dependent uptake of ORMOSIL-FA by HeLa and H1299 cells after 2h treatment in normal RPMI or folate free RPMI. FACS analysis of the FL1 channel signal in respect to theparticles concentration.

For H1299 cell lines at low ORMOSIL-FA concentration (from 5 to 20 µg/ml) the uptake is higher for the structures in folate free medium, but this difference is statistically significant only at a concentration of 5 µg/ml. For HeLa cells at low concentration the uptake is almost the same independently from the presence or not of the external folic acid. Hela cells treated with 40 µg/ml ORMOSIL-FA internalize a larger amount of particles in the absence of free folic acid, that competes for the folic acid receptor binding. On the other hand a folic acid

excess in the external medium doesn't totally inhibit the internalization of the functionalized particles. Only 26.6% of the ORMOSIL-FA uptake can be correlated to the functionalization in the case of H1299 cell treated with 5 µg/ml and 18.4% in the case of HeLa cell treated with 40 µg/ml.

The IC_{50} value obtained from the cell viability experiments as a function of particles concentration are shown in Figure 4.3-6 for HeLa and H1299 cell cultured for 2 h in presence of the ORMOSILs.

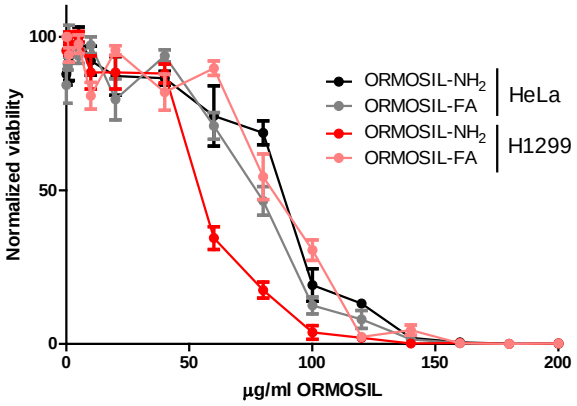

Fig 4.3-6: Dose dependent viability of HeLa and H1299 cells treated with ORMOSIL nanoparticles. Cells were treated for 2h in normal RPMI supplemented with serum and folic acid. Cell viability is obtained though alamar blue® assey.

H1299 are more sensitive to the nude structures than HeLa cell. In detail the IC_{50} value for HeLa cell is 95±5 µg/ml for ORMOSIL-NH_2 and 80±3 µg/ml for ORMOSIL-FA. The IC_{50} value for H1299 cell is, 59±2 µg/ml for ORMOSIL-NH_2 and 61±2 for ORMOSIL-FA.

4.4 Results on Chitosan/pDNA nanoparticles project

Chitosan/plasmid DNA (Chi/pDNA) complex formation has been carried out in sodium acetate buffer 15 mM pH 5.5. In this condition the chitosan amines are protonated and can electrostatically interact with the negatively charged pDNA. The diameter and Z-potential of the formed particles have been measured before the transfection experiments and are reported in Table 4.4-1 for 50kDa Chi/pDNA complex. The Z-potential increases upon increase of the N/P ratio due to the presence of a larger amount of positive chitosan. The J774A-1 macrophage cells have been transfected with Chi/pDNA complexes and also with lipofectamine® and

oligofectamine®, that are known to be two efficient transfecting agents.

Sample 50kDa chitosan	d(nm)	PdI	Z-potential (mV)
NP=2.5	195.0	0.18	19.4
NP=5	167.7	0.37	21.4
NP=10	360.0	0.33	24.2

Tab 4.4-1: Diameter and Z-potential of Chi/pDNA nanoparticles formed using 50 kDa chitosan 100% deacetylated at different N/P ratio with pDNA in Na/acetate buffer pH 5.5.

The transfection efficiency is monitored trough the detection of GFP protein coded by the pDNA used for the complexes production. The experiments have always been negative since expression of GFP in this macrophages cell lines is never observed. The H1299 cells have been then used since they are known to be easily transfected.

The result of H1299 transfection is reported in Figure 4.4-1 for lipofectamine® and oligofectamine®, and Chi/pDNA complex at different N/P ratio

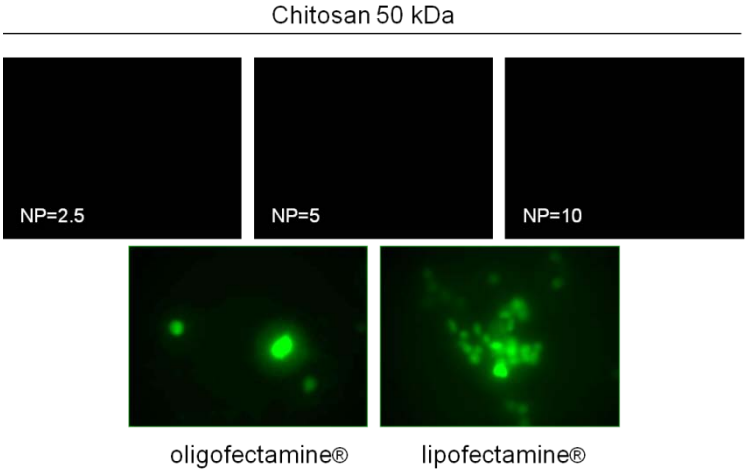

Fig 4.4-1: H1299 cells transfected with the plasmid DNA coding for GFP using Chi/pDNA complex (50kDa chitosan 100% deacetyladed) and lipofectamine® and oligofectamine® transfection agent.

The expression of GFP is never observed for all Chi/pDNA complees tested, while lipofectamine® and oligofectamine® complexes are able to transfect this cell line. Lipofectamine® shows high transfection efficiency,

being the best transfecting agent used. Chi/pDNA complexes fail to transfect H1299 cells, the use of chitosan complex did not yield plasmid expression. To better understand these negative results the ability of Chi/pDNA complexes to cross the cell membrane in macrophages, have been tested at different N/P ratio, using a Cy3 labeled 50kDa chitosan. Fluorescence images have been acquired after 4h and 24h of transfection (Figure 4.4-2) The labeled chitosan signal colocalizes with the brightfield images at 4h of transfection, indicating that chitosan is able to enter the cell. The chitosan signal is still there after 24h from the transfection.

To clarify the the lack of expression, a Cy3-labeled plasmid DNA has been used for Chi/pDNA production, and the Cy3 fluorescent signal has been followed inside the macrophages cell lines after transfection.

In this experiment different ultrapure chitosan oligomers O15, O25 and G214, 100% deacetylated (Novamatrix) and 50kDa chitosan 100% deacetylated in different N/P ratio have been used.

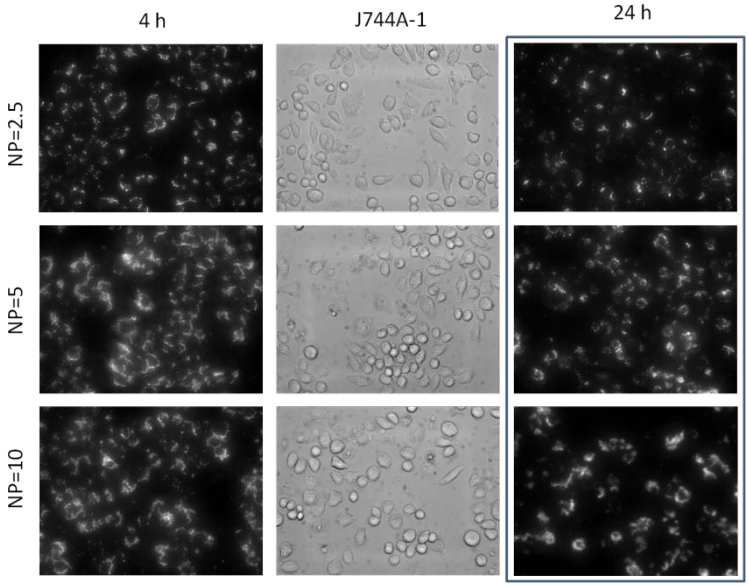

Fig 4.4-2: Chitosan 50 kDa nanoparticles localizatrion in J774A-1 cells, after 4h of transfection (left and central panels) and 1day of transfection (right squared panels) (left panels): Cy3 labeled chitosan after 4h of interactionwith cells The red fluorescence of chitosan is changed in gray scale image. (central panels): Brigthfield images of the left panels Images were acquired with same gate and time exposure and the white signal reflect difference in chitosan concentration for samples with different N/P ratio.

Figures 4.4-3 shows that the red fluorescence of plasmid DNA is inside the J774A-1 cells demonstrating that pDNA is able to cross the cell membrane for all the

chitosan oligomers and the N/P ratio used. The images have been collected in the same conditions, so the intensity of the signal reflects the different amount of pDNA uptaken by cells. It is possible to observe that the amount of delivered pDNA is higer for particles with high N/P ratio or with a longer, due to their more positive Z-value. Despite the chitosan mediated entry of the pDNA into the cells, the plasmid is not expressed, probably due to the high stability of the Chi/pDNA complexes that does not allow the nucleic acid release.

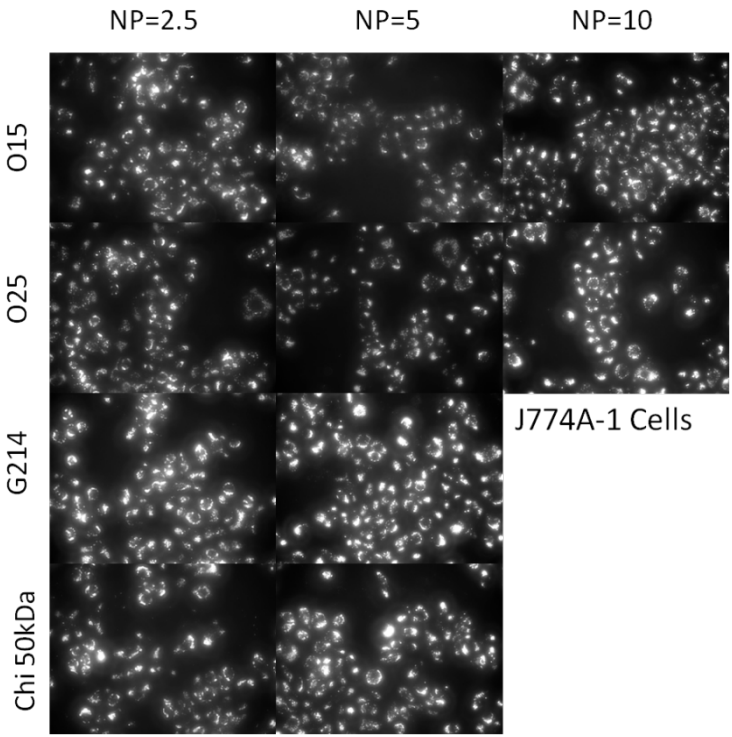

Fig 4.4-4: Plasmid DNA localization in J774A-1 cells, after 1 day of transfection with the plasmid DNA coding for GFP labeled with Cy3. The red fluorescence of Cy3 is changed in gray scale image, the white signal correspond to plasmid labeled DNA.

5. DISCUSSIONS AND CONCLUSIONS

5.1 Discussion on MC-Chi-FA project

In this project, PVA microcapsules have been functionalized with chitosan or chitosan-folate and have been characterized in size distribution and Z-potential. The nude and functionalized capsules have been then characterized for their ability to adsorb and release CPT in presence of different external media. The presence of chitosan or chitosan-folate on MC leads to a drug absorption large than nude MC, likely because of an increased surface area of the functionalized capsules, and of electrostatic interactions between the positively charged chitosan and camptothecin, as confirmed in the release experiment in water and in phosphate buffer (Figures 3.1-7 and 3.1-8). The cumulative CPT release is percentually smaller for MCs loaded with a large amount of drug. This finding permits us to modulate the release of the drug. The drug for the functionalized MC is 2 times slower than for the nude MC in culture medium (Figure 3.1-10a). This effect is reverted in presence of 10% serum in the medium, that accelerates the release

process for all the tested microcapsules (Figure 3.1-10b). MC-Chi-FA are internalized by HeLa cells overexpressing the folate receptor, while no interaction is observed with NIH3t3 fibroblasts used as negative control (Figures 3.1-11). The MC-Chi-FA localization on tumoral HeLa cells is due to the presence of the functionalization with folate as demonstrated by competition experiments in presence of free folic acid in the culture medium that competes for the binding to the receptor. (Figure 3.1-14)

The results of cellular localization fully match the proliferation experiments. Infact, CPT loaded MC-Chi-FA decreases HeLa cells proliferation while they don't perturb the growth of NIH3t3 cells (Figure 3.1-15). These results indicate that microcapsules, modified with chitosan-folate, are a promising system to target camptothecin in tumors of epithelial origin, since the presence of folate permits a selective recognition. Other studies are in progress on different cell lines, also using differently functionalized microbubbles, in the effort to design multivalent therapeutic agents that combine

detectability (using contrast agents for imaging techniques) with tissue specific drug delivery.

5.2 Discussions on MC-Lys-FA project

PVA microcapsules have been functionalized with lysine or lysine folic acid and have been characterized in dimension and surface properties. The structures have been loaded with CPT. MC adsorb around 50% of the external drug solution, while functionalized MC can adsorb 95% of the external drug. The CPT release by the MC-Lys and MC-Lys-FA is 10 times and 5 times respectively slower than the nude MC, also in presence of 10% serum (Figure 3.2-5).

MC-Lys-FA are able to interact with different type of cancer cells of epithelial origin overexpressing the folate receptor, such as HeLa and H1299 cells. The interaction is not observed for NIH3t3 fibroblasts control cells (Figures 3.2-8, 3.2-9 and 3.2-10). An average value of 1.5 and 0.7 MC-Lys-FA /cell is found for HeLa and H1299 cells respectively in absence of free folic acid in the medium (Figure 3.2-11). Also in this case the

interaction is due to the presence of folate on the structure's surface since free folic acid is able to compete with MC-Lys-FA for the binding to FR (Figure 3.2-8 and 3.2-9).

5.3 Discussions on ORMOSIL-FA project

Silica oil-in-water microemulsion have been produced with an uniform shape and size around 70nm and with a negative surface potential of -9.9 and -14.6mV for ORMOSIL-NH_3 and ORMOSIL-FA respectively (Table 3.3-1). The particles can be functionalized with folic acid ($3.75\pm0.35\cdot10^{-8}$ mol FA/mg ORMOSIL-FA), and the conjugation has been used as a strategy to recognize tumor cells expressing FR. ORMOSILs have been internalized by HeLa and H1299 cells, either in presence or in absence of free folic acid. All cell lines internalyze an amount of ORMOSIL-NH_3 larger than ORMOSIL-FA, due to the less negative value of their Z-potential that allow a better interaction with cell membranes. The particles uptake is a saturable process. For H1299 cells, the best effect of the competition is obtained with 5

µg/ml of ORMOSIL-FA, while for HeLa cells is obtained with 40 µg/ml of ORMOSIL-FA (Figure 3.3-5). The folic acid excess in the external medium, used in the competition experiments, doesn't completely inhibit the internalization of the functionalized ORMOSIL, indicating that the interaction is only partially due to the presence of folic acid. Comparison of the amount of particles uptaken in presence or absence of free folate permits to evaluate that only 26% and 18% of the internalized particles, for H1299 cell (treated with 5 µg/ml structures) and HeLa cell (40 µg/ml) respectively, can be ascribed to folic acid functionalization. Measurements of the IC_{50} value (Figure 4.3-6) indicate that ORMOSIL-FA are more biocompatible than ORMOSIL-NH_3 on H1299 cells. However the larger IC_{50} value, corresponding to 95±5 µg/ml, is still low to consider the ORMOSILs fully biocompatible. As a general comment we can say that the structures are not biocompatible, not only for the toxicity in the micro-molar range but also for the short time (2h), required to give toxicity. The toxicity can be attributed to the

contamination with surfactant (Aerosol-OT) used during the synthesis procedure, since this surfactant is reported to be toxic at a concentration around 30 µM (Roy *et al*, 2005).

5.4 Discussions on Chitosan/pDNA nanoparticles project.

Chitosan/plasmid DNA (Chi/pDNA) complex formation is due to electrostatic interaction between the negatively charged pDNA and the positive chitosan. The diameter and Z-potential of the complexes is proportional to the N/P ratio. Chi/pDNA, lipofectamine® and oligofectamine® complexes are not able to transfect J774A-1 macrophage cell line, since no GFP expression is observed. The GFP expression has been observed in H1299 cells using the standard transfection agents lipofectamine® and oligofectamine® (Figure 3.4-1), while chitosan is not able to grant the expression of pDNA in H1299 control cells. Fluorescence microscopy studies, using Cy3 labeled 50kDa chitosan and pDNA, indicate

that Chi/pDNA complexes localize into the cells after 4 h of transfection without inducing the plasmid expression.

We hypothesize that the Chi/pDNA complexes are very stable, so that the pDNA is not released in the cytosol and is not transcripted and translated in to the GFP protein. Measurements of the stability of these structures are under progress, to clarify the best strategy to destabilize the Chi/pDNA complexes.

REFERENCES

Adiga, S.P., Jin, C., Curtiss, L.A., Monteiro-Riviere, N.A., and Narayan, R.J. (2009). Nanoporous membranes for medical and biological applications. Wiley Interdiscip Rev Nanomed Nanobiotechnol *1*, 568–581.

Anderson, R.G. (1993). Caveolae: where incoming and outgoing messengers meet. Proc. Natl. Acad. Sci. U.S.A. *90*, 10909–10913.

Anderson, R.G., Kamen, B.A., Rothberg, K.G., and Lacey, S.W. (1992). Potocytosis: sequestration and transport of small molecules by caveolae. Science *255*, 410–411.

Antony, A.C. (1992). The biological chemistry of folate receptors. Blood *79*, 2807–2820.

Antony, A.C. (1996). Folate receptors. Annu. Rev. Nutr. *16*, 501–521.

Antony, A.C., Briddell, R.A., Brandt, J.E., Straneva, J.E.,

Verma, R.S., Miller, M.E., Kalasinski, L.A., and Hoffman, R. (1991). Megaloblastic hematopoiesis in vitro. Interaction of anti-folate receptor antibodies with hematopoietic progenitor cells leads to a proliferative response independent of megaloblastic changes. J. Clin. Invest. *87*, 313–325.

Artursson, P., Lindmark, T., Davis, S.S., and Illum, L. (1994). Effect of chitosan on the permeability of monolayers of intestinal epithelial cells (Caco-2). Pharm. Res. *11*, 1358–1361.

Bases Jr, C.-F., and Mesner, R.-E. (1974). The hydrolysis of cations. Wiley New York

Bakhshandeh, H., Soleimani, M., Hosseini, S.S., Hashemi, H., Shabani, I., Shafiee, A., Nejad, A.H.B., Erfan, M., Dinarvand, R., and Atyabi, F. (2011). Poly (ε-caprolactone) nanofibrous ring surrounding a polyvinyl alcohol hydrogel for the development of a biocompatible two-part artificial cornea. Int J Nanomedicine *6*, 1509–1515.

Bangham, A.D. (1993). Liposomes: the Babraham connection. Chem. Phys. Lipids *64*, 275–285.

Bangham, A.D., Standish, M.M., and Miller, N. (1965). Cation permeability of phospholipid model membranes: effect of narcotics. Nature *208*, 1295–1297.

Bangham, A.D., Standish, M.M., and Watkins, J.C. (1965). Diffusion of univalent ions across the lamellae of swollen phospholipids. J. Mol. Biol. *13*, 238–252.

Bannon, M., Kapatos, G., and Albertson, D. (2005). Gene expression profiling in the brains of human cocaine abusers. Addict Biol *10*, 119–126.

Benmerah, A., Bayrou, M., Cerf-Bensussan, N., and Dautry-Varsat, A. (1999). Inhibition of clathrin-coated pit assembly by an Eps15 mutant. J. Cell. Sci. *112 (Pt 9)*, 1303–1311.

Bharali, D.J., Klejbor, I., Stachowiak, E.K., Dutta, P., Roy, I., Kaur, N., Bergey, E.J., Prasad, P.N., and Stachowiak, M.K. (2005). Organically modified silica

nanoparticles: a nonviral vector for in vivo gene delivery and expression in the brain. Proc. Natl. Acad. Sci. U.S.A. *102*, 11539–11544.

Bhaskar, S., Tian, F., Stoeger, T., Kreyling, W., de la Fuente, J.M., Grazú, V., Borm, P., Estrada, G., Ntziachristos, V., and Razansky, D. (2010). Multifunctional Nanocarriers for diagnostics, drug delivery and targeted treatment across blood-brain barrier: perspectives on tracking and neuroimaging. Part Fibre Toxicol *7*, 3.

Boucher, Y., Baxter, L.T., and Jain, R.K. (1990). Interstitial pressure gradients in tissue-isolated and subcutaneous tumors: implications for therapy. Cancer Res. *50*, 4478–4484.

Bruchez, M., Jr, Moronne, M., Gin, P., Weiss, S., and Alivisatos, A.P. (1998). Semiconductor nanocrystals as fluorescent biological labels. Science *281*, 2013–2016.

Bullock, P., Champoux, J.J., and Botchan, M. (1985). Association of crossover points with topoisomerase I

cleavage sites: a model for nonhomologous recombination. Science *230*, 954–958.

Burns, A., Ow, H., and Wiesner, U. (2006). Fluorescent core-shell silica nanoparticles: towards “Lab on a Particle” architectures for nanobiotechnology. Chem Soc Rev *35*, 1028–1042.

Cavalieri, F., Chiessi, E., Finelli, I., Natali, F., Paradossi, G., and Telling, M.F. (2006). Water, solute, and segmental dynamics in polysaccharide hydrogels. Macromol Biosci *6*, 579–589.

Cavalieri, F., El Hamassi, A., Chiessi, E., and Paradossi, G. (2005). Stable polymeric microballoons as multifunctional device for biomedical uses: synthesis and characterization. Langmuir *21*, 8758–8764.

Champoux, J.J. (2001). DNA topoisomerases: structure, function, and mechanism. Annu. Rev. Biochem. *70*, 369–413.

Chang, W.J., Rothberg, K.G., Kamen, B.A., and

Anderson, R.G. (1992). Lowering the cholesterol content of MA104 cells inhibits receptor-mediated transport of folate. J. Cell Biol. *118*, 63–69.

Chen, J., Li, S., Shen, Q., He, H., and Zhang, Y. (2011). Enhanced cellular uptake of folic acid-conjugated PLGA-PEG nanoparticles loaded with vincristine sulfate in human breast cancer. Drug Dev Ind Pharm *37*, 1339–1346.

Chen, X., Park, R., Shahinian, A.H., Bading, J.R., and Conti, P.S. (2004). Pharmacokinetics and tumor retention of 125I-labeled RGD peptide are improved by PEGylation. Nucl. Med. Biol. *31*, 11–19.

Cho, H.S., Lee, H.H., Choi, S.J., Kim, K.J., Jeun, S.H., Li, Q.-Z., and Sung, K.-W. (2008). Forskolin Enhances Synaptic Transmission in Rat Dorsal Striatum through NMDA Receptors and PKA in Different Phases. Korean J. Physiol. Pharmacol. *12*, 293–297.

Choi, C.H.J., Alabi, C.A., Webster, P., and Davis, M.E. (2010). Mechanism of active targeting in solid tumors

with transferrin-containing gold nanoparticles. Proc. Natl. Acad. Sci. U.S.A. *107*, 1235–1240.

Choi, H., Choi, S.R., Zhou, R., Kung, H.F., and Chen, I.-W. (2004). Iron oxide nanoparticles as magnetic resonance contrast agent for tumor imaging via folate receptor-targeted delivery. Acad Radiol *11*, 996–1004.

Clark, H.A., Hoyer, M., Philbert, M.A., and Kopelman, R. (1999). Optical nanosensors for chemical analysis inside single living cells. 1. Fabrication, characterization, and methods for intracellular delivery of PEBBLE sensors. Anal. Chem. *71*, 4831–4836.

Coney, L.R., Tomassetti, A., Carayannopoulos, L., Frasca, V., Kamen, B.A., Colnaghi, M.I., and Zurawski, V.R., Jr (1991). Cloning of a tumor-associated antigen: MOv18 and MOv19 antibodies recognize a folate-binding protein. Cancer Res. *51*, 6125–6132.

Coradin, T., and Lopez, P.J. (2003). Biogenic silica patterning: simple chemistry or subtle biology? Chembiochem *4*, 251–259.

Cricenti, A., and Generosi, R. (1995). Air operating atomic force-scanning tunneling microscope suitable to study semiconductors, metals, and biological samples. Review of Scientific Instruments *66*, 2843.

Cui, D., Tian, F., Coyer, S.R., Wang, J., Pan, B., Gao, F., He, R., and Zhang, Y. (2007). Effects of antisense-myc-conjugated single-walled carbon nanotubes on HL-60 cells. J Nanosci Nanotechnol *7*, 1639–1646.

Cui, D., Tian, F., Kong, Y., Ozkan, C., Titushikin, I., and Gao, H. (2004). Effects of single-walled carbon nanotubes on the polymerase chain reaction. Nanotechnology. *1*, 154-157.

Dai, T., Tanaka, M., Huang, Y.-Y., and Hamblin, M.R. (2011). Chitosan preparations for wounds and burns: antimicrobial and wound-healing effects. Expert Rev Anti Infect Ther *9*, 857–879.

Dalla Palma, L., and Bertolotto, M. (1999). Introduction to ultrasound contrast agents: physics overview. Eur

Radiol *9 Suppl 3*, S338–S342.

Davis, M.E., Chen, Z.G., and Shin, D.M. (2008). Nanoparticle therapeutics: an emerging treatment modality for cancer. Nat Rev Drug Discov *7*, 771–782.

De la Isla, A., Brostow, W., Bujard, B., Estevez, M., Rodriguez, J.R., Vargas, S., and Castaño, V.M. (2003). Nanohybrid scratch resistant coatings for teeth and bone viscoelasticity manifested in tribology. Materials Research Innovations. *2*, 110-114.

Deng, T.S., Zhang, Q.F., Zhang, J.Y., Shen, X., Zhu, K.T., and Wu, J.L. (2009). One-step synthesis of highly monodisperse hybrid silica spheres in aqueous solution. J Colloid Interface Sci *329*, 292–299.

Dixon, K.H., Lanpher, B.C., Chiu, J., Kelley, K., and Cowan, K.H. (1994). A novel cDNA restores reduced folate carrier activity and methotrexate sensitivity to transport deficient cells. J. Biol. Chem. *269*, 17–20.

Dixon, K.H., Mulligan, T., Chung, K.N., Elwood, P.C., and Cowan, K.H. (1992). Effects of folate receptor expression following stable transfection into wild type and methotrexate transport-deficient ZR-75-1 human breast cancer cells. J. Biol. Chem. *267*, 24140–24147.

Dubey, P.K., Mishra, V., Jain, S., Mahor, S., and Vyas, S.P. (2004). Liposomes modified with cyclic RGD peptide for tumor targeting. J Drug Target *12*, 257–264.

Duncan, R. (2003a). The dawning era of polymer therapeutics. Nat Rev Drug Discov *2*, 347–360.

Edelstein, R.L., Tamanaha, C.R., Sheehan, P.E., Miller, M.M., Baselt, D.R., Whitman, L.J., and Colton, R.J. (2000). The BARC biosensor applied to the detection of biological warfare agents. Biosens Bioelectron *14*, 805–813.

Fadeel, B., and Garcia-Bennett, A.E. (2010). Better safe than sorry: Understanding the toxicological properties of inorganic nanoparticles manufactured for biomedical applications. Adv. Drug Deliv. Rev. *62*, 362–374.

Fassberg, J., and Stella, V.J. (1992). A kinetic and mechanistic study of the hydrolysis of camptothecin and some analogues. J Pharm Sci *81*, 676–684.

Ferraretto, A., Sonnino, S., Soria, M.R., and Masserini, M. (1996). Characterization of biotinylated liposomes sensitive to temperature and pH: new tools for anti-cancer drug delivery. Chem. Phys. Lipids *82*, 133–139.

Ferrari, M. (2005). Cancer nanotechnology: opportunities and challenges. Nat. Rev. Cancer *5*, 161–171.

Ferrari, M. (2005). Nanovector therapeutics. Curr Opin Chem Biol *9*, 343–346.

Fu, C., Sun, X., Liu, D., Chen, Z., Lu, Z., and Zhang, N. (2011). Biodegradable Tri-Block Copolymer Poly(lactic acid)-poly(ethylene glycol)-poly(l-lysine)(PLA-PEG-PLL) as a Non-Viral Vector to Enhance Gene Transfection. Int J Mol Sci *12*, 1371–1388.

Gabizon, A., Shmeeda, H., Horowitz, A.T., and Zalipsky, S. (2004). Tumor cell targeting of liposome-entrapped

drugs with phospholipid-anchored folic acid-PEG conjugates. Adv. Drug Deliv. Rev. *56*, 1177–1192.

Galbiati, A., Tabolacci, C., Turcano, L., Cienciarelli, O., Morozzo Della Rocca, B., Beninati, S., Paradossi, G., and Desideri, A. (2010). Chitosan-folate modified microcapsules specifically target tumor cells. Poster section ANIS2, Alp Nano Bio.

Garcia-Carbonero, R., and Supko, J.G. (2002). Current perspectives on the clinical experience, pharmacology, and continued development of the camptothecins. Clin. Cancer Res. *8*, 641–661.

Geng, H., Song, H., Qi, J., and Cui, D. (2011). Sustained release of VEGF from PLGA nanoparticles embedded thermo-sensitive hydrogel in full-thickness porcine bladder acellular matrix. Nanoscale Res Lett *6*, 312.

Gilmour, D.S., and Elgin, S.C. (1987). Association of topoisomerase I with transcriptionally active loci in Drosophila. NCI Monogr 17–21.

Gindy, M.E., and Prud'homme, R.K. (2009). Multifunctional nanoparticles for imaging, delivery and targeting in cancer therapy. Expert Opin Drug Deliv *6*, 865–878.

Gordon, A.N., Fleagle, J.T., Guthrie, D., Parkin, D.E., Gore, M.E., and Lacave, A.J. (2001). Recurrent epithelial ovarian carcinoma: a randomized phase III study of pegylated liposomal doxorubicin versus topotecan. J. Clin. Oncol. *19*, 3312–3322.

Gradishar, W.J., Tjulandin, S., Davidson, N., Shaw, H., Desai, N., Bhar, P., Hawkins, M., and O'Shaughnessy, J. (2005). Phase III trial of nanoparticle albumin-bound paclitaxel compared with polyethylated castor oil-based paclitaxel in women with breast cancer. J. Clin. Oncol. *23*, 7794–7803.

Han, L., Huang, R., Liu, S., Huang, S., and Jiang, C. (2010). Peptide-conjugated PAMAM for targeted doxorubicin delivery to transferrin receptor overexpressed tumors. Mol. Pharm. *7*, 2156–2165.

Harvey, C.J., Blomley, M.J., Eckersley, R.J., and Cosgrove, D.O. (2001). Developments in ultrasound contrast media. Eur Radiol *11*, 675–689.

Henderson, G.I., Perez, T., Schenker, S., Mackins, J., and Antony, A.C. (1995). Maternal-to-fetal transfer of 5-methyltetrahydrofolate by the perfused human placental cotyledon: evidence for a concentrative role by placental folate receptors in fetal folate delivery. J. Lab. Clin. Med. *126*, 184–203.

He, Q., Gao, Y., Zhang, L., Zhang, Z., Gao, F., Ji, X., Li, Y., and Shi, J. (2011). A pH-responsive mesoporous silica nanoparticles-based multi-drug delivery system for overcoming multi-drug resistance. Biomaterials *32*, 7711–7720.

Hernot, S., and Klibanov, A.L. (2008). Microbubbles in ultrasound-triggered drug and gene delivery. Adv. Drug Deliv. Rev. *60*, 1153–1166.

Higuchi, Y., Kawakami, S., and Hashida, M. (2010). Strategies for in vivo delivery of siRNAs: recent

progress. BioDrugs *24*, 195–205.

Howard, K.A., Dong, M., Oupicky, D., Bisht, H.S., Buss, C., Besenbacher, F., and Kjems, J. (2007). Nanocarrier stimuli-activated gene delivery. Small *3*, 54–57.

Howard, K.A., Paludan, S.R., Behlke, M.A., Besenbacher, F., Deleuran, B., and Kjems, J. (2009). Chitosan/siRNA nanoparticle-mediated TNF-alpha knockdown in peritoneal macrophages for anti-inflammatory treatment in a murine arthritis model. Mol. Ther. *17*, 162–168.

Hsiang, Y.H., Hertzberg, R., Hecht, S., and Liu, L.F. (1985). Camptothecin induces protein-linked DNA breaks via mammalian DNA topoisomerase I. J. Biol. Chem. *260*, 14873–14878.

Hsiang, Y.H., Wu, H.Y., and Liu, L.F. (1988). Proliferation-dependent regulation of DNA topoisomerase II in cultured human cells. Cancer Res. *48*, 3230–3235.

Huang, R.K., Steinmetz, N.F., Fu, C.-Y., Manchester, M., and Johnson, J.E. (2011). Transferrin-mediated targeting of bacteriophage HK97 nanoparticles into tumor cells. Nanomedicine (Lond) *6*, 55–68.

Huh, D., Mills, K.L., Zhu, X., Burns, M.A., Thouless, M.D., and Takayama, S. (2007). Tuneable elastomeric nanochannels for nanofluidic manipulation. Nat Mater *6*, 424–428.

Huynh, T.T.N., Padois, K., Sonvico, F., Rossi, A., Zani, F., Pirot, F., Doury, J., and Falson, F. (2010). Characterization of a polyurethane-based controlled release system for local delivery of chlorhexidine diacetate. Eur J Pharm Biopharm *74*, 255–264.

Illum, L. (1998). Chitosan and its use as a pharmaceutical excipient. Pharm. Res. *15*, 1326–1331.

Illum, L. (2003). Nasal drug delivery--possibilities, problems and solutions. J Control Release *87*, 187–198.

Jain, K.K. (2010). Advances in the field of

nanooncology. BMC Med *8*, 83.

Jain, R.K. (1987). Transport of molecules in the tumor interstitium: a review. Cancer Res. *47*, 3039–3051.

Jain, R.K. (1989). Delivery of novel therapeutic agents in tumors: physiological barriers and strategies. J. Natl. Cancer Inst. *81*, 570–576.

Jain, R.K. (2001). Delivery of molecular and cellular medicine to solid tumors. Adv. Drug Deliv. Rev. *46*, 149–168.

Jain, R.K. (2005). Normalization of tumor vasculature: an emerging concept in antiangiogenic therapy. Science *307*, 58–62.

Jain, R.K., and Stylianopoulos, T. (2010). Delivering nanomedicine to solid tumors. Nat Rev Clin Oncol *7*, 653–664.

Kamen, B.A., Smith, A.K., and Anderson, R.G. (1991). The folate receptor works in tandem with a probenecid-

sensitive carrier in MA104 cells in vitro. J. Clin. Invest. *87*, 1442–1449.

Kim, B.Y.S., Rutka, J.T., and Chan, W.C.W. (2010). Nanomedicine. N. Engl. J. Med. *363*, 2434–2443.

Kim, W.J., and Kim, S.W. (2009). Efficient siRNA delivery with non-viral polymeric vehicles. Pharm. Res. *26*, 657–666.

Kim, S., Huang, H., Pudavar, H. E., Cui, Y. P., and Prasad, P. N. (2007). Intraparticle energy transfer and fluorescence photoconversion in nanoparticles: an optical highlighter nanoprobe for two-photon bioimaging. Chem. Mater. *19*, 5650-5656

Kim, S., Pudavar, H. E., Bonoiu, A., and Prasad, P. N. (2007). Aggregation-enhanced fluorescence in organically modified silica nanoparticles: a novel approach toward high-signal-output nanoprobes for two-photon fluorescence bioimaging. Adv. Mater. *19*, 3791-3795.

Kingsbury, W.D., Boehm, J.C., Jakas, D.R., Holden, K.G., Hecht, S.M., Gallagher, G., Caranfa, M.J., McCabe, F.L., Faucette, L.F., and Johnson, R.K. (1991). Synthesis of water-soluble (aminoalkyl)camptothecin analogues: inhibition of topoisomerase I and antitumor activity. J. Med. Chem. *34*, 98–107.

Koning, G.A., Fretz, M.M., Woroniecka, U., Storm, G., and Krijger, G.C. (2004). Targeting liposomes to tumor endothelial cells for neutron capture therapy. Appl Radiat Isot *61*, 963–967.

Kopecek, J., Kopecková, P., Minko, T., and Lu, Z. (2000). HPMA copolymer-anticancer drug conjugates: design, activity, and mechanism of action. Eur J Pharm Biopharm *50*, 61–81.

Koster, D.A., Croquette, V., Dekker, C., Shuman, S., and Dekker, N.H. (2005). Friction and torque govern the relaxation of DNA supercoils by eukaryotic topoisomerase IB. Nature *434*, 671–674.

Kularatne, S.A., and Low, P.S. (2010). Targeting of

nanoparticles: folate receptor. Methods Mol. Biol. *624*, 249–265.

Köping-Höggård, M., Tubulekas, I., Guan, H., Edwards, K., Nilsson, M., Vårum, K.M., and Artursson, P. (2001). Chitosan as a nonviral gene delivery system. Structure-property relationships and characteristics compared with polyethylenimine in vitro and after lung administration in vivo. Gene Ther. *8*, 1108–1121.

Leamon, C.P., and Low, P.S. (1991). Delivery of macromolecules into living cells: a method that exploits folate receptor endocytosis. Proc. Natl. Acad. Sci. U.S.A. *88*, 5572–5576.

Lencioni, R., Cioni, D., and Bartolozzi, C. (2002). Tissue harmonic and contrast-specific imaging: back to gray scale in ultrasound. Eur Radiol *12*, 151–165.

Leppard, J.B., and Champoux, J.J. (2005). Human DNA topoisomerase I: relaxation, roles, and damage control. Chromosoma *114*, 75–85.

Leteurtre, F., Fesen, M., Kohlhagen, G., Kohn, K.W., and Pommier, Y. (1993). Specific interaction of camptothecin, a topoisomerase I inhibitor, with guanine residues of DNA detected by photoactivation at 365 nm. Biochemistry *32*, 8955–8962.

Liu, C., Pouliot, J.J., and Nash, H.A. (2002). Repair of topoisomerase I covalent complexes in the absence of the tyrosyl-DNA phosphodiesterase Tdp1. Proc. Natl. Acad. Sci. U.S.A. *99*, 14970–14975.

Liu, J., Qiao, S.Z., Hu, Q.H., and Lu, G.Q.M. (2011). Magnetic nanocomposites with mesoporous structures: synthesis and applications. Small *7*, 425–443.

Liu, X., Howard, K.A., Dong, M., Andersen, M.Ø., Rahbek, U.L., Johnsen, M.G., Hansen, O.C., Besenbacher, F., and Kjems, J. (2007). The influence of polymeric properties on chitosan/siRNA nanoparticle formulation and gene silencing. Biomaterials *28*, 1280–1288.

Lu, T., Sun, J., Chen, X., Zhang, P., and Jing, X. (2009).

Folate-conjugated micelles and their folate-receptor-mediated endocytosis. Macromol Biosci *9*, 1059–1068.

Löbenberg, R., and Amidon, G.L. (2000). Modern bioavailability, bioequivalence and biopharmaceutics classification system. New scientific approaches to international regulatory standards. Eur J Pharm Biopharm *50*, 3–12.

Maeda, H., Wu, J., Sawa, T., Matsumura, Y., and Hori, K. (2000). Tumor vascular permeability and the EPR effect in macromolecular therapeutics: a review. J Control Release *65*, 271–284.

Ma, J., Huifen, W., Kong, L.-B., Peng, K.-W. (2003). Biomimetic processing of nanocrystallite bioactive apatite coating on titanium. Nanotechnology. *14*, 619-623.

Mao, S., Sun, W., and Kissel, T. (2010). Chitosan-based formulations for delivery of DNA and siRNA. Adv. Drug Deliv. Rev. *62*, 12–27.

Masserini, M., Palestini, P., Pitto, M., Chigorno, V., and

Sonnino, S. (2002). Preparation and use of liposomes for the study of sphingolipid segregation in membrane model systems. Methods Mol. Biol. *199*, 17–27.

Matsumura, Y., and Maeda, H. (1986). A new concept for macromolecular therapeutics in cancer chemotherapy: mechanism of tumoritropic accumulation of proteins and the antitumor agent smancs. Cancer Res. *46*, 6387–6392.

Maul, G.G., French, B.T., van Venrooij, W.J., and Jimenez, S.A. (1986). Topoisomerase I identified by scleroderma 70 antisera: enrichment of topoisomerase I at the centromere in mouse mitotic cells before anaphase. Proc. Natl. Acad. Sci. U.S.A. *83*, 5145–5149.

Mayor, S., Rothberg, K.G., and Maxfield, F.R. (1994). Sequestration of GPI-anchored proteins in caveolae triggered by cross-linking. Science *264*, 1948–1951.

Mel'nikova, Y.S., Mel'nikov, S.M., and Löfroth, J.E. (1999). Physico-chemical aspects of the interaction between DNA and oppositely charged mixed liposomes. Biophys. Chem. *81*, 125–141.

Miotti, S., Facheris, P., Tomassetti, A., Bottero, F., Bottini, C., Ottone, F., Colnaghi, M.I., Bunni, M.A., Priest, D.G., and Canevari, S. (1995). Growth of ovarian-carcinoma cell lines at physiological folate concentration: effect on folate-binding protein expression in vitro and in vivo. Int. J. Cancer *63*, 395–401.

Moghimi, S.M., Hunter, A.C., and Murray, J.C. (2005). Nanomedicine: current status and future prospects. FASEB J. *19*, 311–330.

Molday, R.S., and MacKenzie, D. (1982). Immunospecific ferromagnetic iron-dextran reagents for the labeling and magnetic separation of cells. J. Immunol. Methods *52*, 353–367.

Moradi, M., Tajik, H., Razavi Rohani, S.M., and Oromiehie, A.R. (2011). Effectiveness of Zataria multiflora Boiss essential oil and grape seed extract impregnated chitosan film on ready-to-eat mortadella-type sausages during refrigerated storage. Journal of the Science of Food and Agriculture.

Mo, Y.Y., Wang, P., and Beck, W.T. (2000). Functional expression of human DNA topoisomerase I and its subcellular localization in HeLa cells. Exp. Cell Res. *256*, 480–490.

Nam, J.-M., Thaxton, C.S., and Mirkin, C.A. (2003). Nanoparticle-based bio-bar codes for the ultrasensitive detection of proteins. Science *301*, 1884–1886.

Neu, M., Fischer, D., and Kissel, T. (2005). Recent advances in rational gene transfer vector design based on poly(ethylene imine) and its derivatives. J Gene Med *7*, 992–1009.

Nguyen, S., Alund, S.J., Hiorth, M., Kjøniksen, A.-L., and Smistad, G. (2011). Studies on pectin coating of liposomes for drug delivery. Colloids Surf B Biointerfaces *88*, 664–673.

Ni, S., Stephenson, S.M., and Lee, R.J. (2002). Folate receptor targeted delivery of liposomal daunorubicin into tumor cells. Anticancer Res. *22*, 2131–2135.

Noguchi, Y., Wu, J., Duncan, R., Strohalm, J., Ulbrich, K., Akaike, T., and Maeda, H. (1998). Early phase tumor accumulation of macromolecules: a great difference in clearance rate between tumor and normal tissues. Jpn. J. Cancer Res. *89*, 307–314.

Nori, A., and Kopecek, J. (2005). Intracellular targeting of polymer-bound drugs for cancer chemotherapy. Adv. Drug Deliv. Rev. *57*, 609–636.

O'Connor, P.M., Nieves-Neira, W., Kerrigan, D., Bertrand, R., Goldman, J., Kohn, K.W., and Pommier, Y. (1991). S-phase population analysis does not correlate with the cytotoxicity of camptothecin and 10,11-methylenedioxycamptothecin in human colon carcinoma HT-29 cells. Cancer Commun. *3*, 233–240.

Ohulchanskyy, T.Y., Roy, I., Goswami, L.N., Chen, Y., Bergey, E.J., Pandey, R.K., Oseroff, A.R., and Prasad, P.N. (2007). Organically modified silica nanoparticles with covalently incorporated photosensitizer for photodynamic therapy of cancer. Nano Lett. *7*, 2835–

2842.

Padula, C., Nicoli, S., Aversa, V., Colombo, P., Falson, F., Pirot, F., and Santi, P. (2007). Bioadhesive film for dermal and transdermal drug delivery. Eur J Dermatol *17*, 309–312.

Pan, D., Turner, J.L., and Wooley, K.L. (2003). Folic acid-conjugated nanostructured materials designed for cancer cell targeting. Chem. Commun. (Camb.) 2400–2401.

Pantarotto, D., Partidos, C.D., Hoebeke, J., Brown, F., Kramer, E., Briand, J.-P., Muller, S., Prato, M., and Bianco, A. (2003). Immunization with peptide-functionalized carbon nanotubes enhances virus-specific neutralizing antibody responses. Chem. Biol. *10*, 961–966.

Parak. W., Boudreau, R., Gros, M.-L., Gerion, D., Zanchet, D., Micheel, C., Williams, S., Alivisatos, A.-P., and Larabell, C. (2002). Cell motility and metastatic

potential studies based on quantum dot imaging of phagokinetic tracks. Advanced Materials. *12*, 882-885.

Pizzolato, J.F., and Saltz, L.B. (2003). The camptothecins. Lancet *361*, 2235–2242.

Pommier, Y. (2006). Topoisomerase I inhibitors: camptothecins and beyond. Nat. Rev. Cancer *6*, 789–802.

Prasad, P.D., Mahesh, V.B., Leibach, F.H., and Ganapathy, V. (1994). Functional coupling between a bafilomycin A1-sensitive proton pump and a probenecid-sensitive folate transporter in human placental choriocarcinoma cells. Biochim. Biophys. Acta *1222*, 309–314.

Qian, J., Li, X., Wei, M., Gao, X., Xu, Z., and He, S. (2008). Bio-molecule-conjugated fluorescent organically modified silica nanoparticles as optical probes for cancer cell imaging. Opt Express *16*, 19568–19578.

Redinbo, M.R., Stewart, L., Kuhn, P., Champoux, J.J., and Hol, W.G. (1998). Crystal structures of human

topoisomerase I in covalent and noncovalent complexes with DNA. Science *279*, 1504–1513.

Ribeiro, M.P., Espiga, A., Silva, D., Baptista, P., Henriques, J., Ferreira, C., Silva, J.C., Borges, J.P., Pires, E., Chaves, P., et al. (2009). Development of a new chitosan hydrogel for wound dressing. Wound Repair Regen *17*, 817–824.

Ross, J.F., Chaudhuri, P.K., and Ratnam, M. (1994). Differential regulation of folate receptor isoforms in normal and malignant tissues in vivo and in established cell lines. Physiologic and clinical implications. Cancer *73*, 2432–2443.

Ross, J.F., Wang, H., Behm, F.G., Mathew, P., Wu, M., Booth, R., and Ratnam, M. (1999). Folate receptor type beta is a neutrophilic lineage marker and is differentially expressed in myeloid leukemia. Cancer *85*, 348–357.

Roy, I., Ohulchanskyy, T.Y., Bharali, D.J., Pudavar, H.E., Mistretta, R.A., Kaur, N., and Prasad, P.N. (2005). Optical tracking of organically modified silica

nanoparticles as DNA carriers: a nonviral, nanomedicine approach for gene delivery. Proc. Natl. Acad. Sci. U.S.A. *102*, 279–284.

Roy, I., Ohulchanskyy, T.Y., Pudavar, H.E., Bergey, E.J., Oseroff, A.R., Morgan, J., Dougherty, T.J., and Prasad, P.N. (2003). Ceramic-based nanoparticles entrapping water-insoluble photosensitizing anticancer drugs: a novel drug-carrier system for photodynamic therapy. J. Am. Chem. Soc. *125*, 7860–7865.

Sabharanjak, S., Sharma, P., Parton, R.G., and Mayor, S. (2002). GPI-anchored proteins are delivered to recycling endosomes via a distinct cdc42-regulated, clathrin-independent pinocytic pathway. Dev. Cell *2*, 411–423.

Sachdeva, M.S. (1998). Drug targeting systems for cancer chemotherapy. Expert Opin Investig Drugs *7*, 1849–1864.

Sahoo, S.K., Parveen, S., and Panda, J.J. (2007). The present and future of nanotechnology in human health care. Nanomedicine *3*, 20–31.

Schipper, N.G., Vårum, K.M., and Artursson, P. (1996). Chitosans as absorption enhancers for poorly absorbable drugs. 1: Influence of molecular weight and degree of acetylation on drug transport across human intestinal epithelial (Caco-2) cells. Pharm. Res. *13*, 1686–1692.

Schoeffler, A.J., and Berger, J.M. (2008). DNA topoisomerases: harnessing and constraining energy to govern chromosome topology. Q. Rev. Biophys. *41*, 41–101.

Schroeder, A., Levins, C.G., Cortez, C., Langer, R., and Anderson, D.G. (2010). Lipid-based nanotherapeutics for siRNA delivery. J. Intern. Med. *267*, 9–21.

Schraa, A.J., Kok, R.J., Moorlag, H.E., Bos, E.J., Proost, J.H., Meijer, D.K.F., de Leij, L.F.M.H., and Molema, G. (2002). Targeting of RGD-modified proteins to tumor vasculature: a pharmacokinetic and cellular distribution study. Int. J. Cancer *102*, 469–475.

Scott, D.W., and De Groot, A.S. (2010). Can we prevent immunogenicity of human protein drugs? Ann. Rheum.

Dis. *69 Suppl 1*, i72–i76.

Selvan, S.T., Tan, T.T.Y., Yi, D.K., and Jana, N.R. (2010). Functional and multifunctional nanoparticles for bioimaging and biosensing. Langmuir *26*, 11631–11641.

Shelma, R., and Sharma, C.P. (2011). Submicroparticles composed of amphiphilic chitosan derivative for oral insulin and curcumin release applications. Colloids Surf B Biointerfaces *88*, 722–728.

Shen, F., Ross, J.F., Wang, X., and Ratnam, M. (1994). Identification of a novel folate receptor, a truncated receptor, and receptor type beta in hematopoietic cells: cDNA cloning, expression, immunoreactivity, and tissue specificity. Biochemistry *33*, 1209–1215.

Shimada, M., Natsugoe, S., and Aikou, T. (1995). Enhanced efficacy of Bleomycin adsorbed on silica particles against lymph node metastasis derived from a transplanted tumor. Anticancer Res. *15*, 109–115.

Shim, M.S., and Kwon, Y.J. (2010). Efficient and

targeted delivery of siRNA in vivo. FEBS J. *277*, 4814–4827.

Shinkai, M., Ueda, K., Ohtsu, S., Honda, H., Kohri, K., and Kobayashi, T. (1999). Effect of functional magnetic particles on radiofrequency capacitive heating. Jpn J Cancer Res. *6*, 699-704.

Singh, M.N., Yadav, H.K.S., Ram, M., and Shivakumar, H.G. (2011). Freeze Dried Chitosan/ Poly-(Glutamic Acid) Microparticles for Intestinal Delivery of Lansoprazole. Current Drug Delivery.

Spinella, M.J., Brigle, K.E., Sierra, E.E., and Goldman, I.D. (1995). Distinguishing between folate receptor-alpha-mediated transport and reduced folate carrier-mediated transport in L1210 leukemia cells. J. Biol. Chem. *270*, 7842–7849.

Stewart, L., Ireton, G.C., and Champoux, J.J. (1997). Reconstitution of human topoisomerase I by fragment complementation. J. Mol. Biol. *269*, 355–372.

Stewart, L., Redinbo, M.R., Qiu, X., Hol, W.G., and Champoux, J.J. (1998). A model for the mechanism of human topoisomerase I. Science *279*, 1534–1541.

Strumberg, D., Pilon, A.A., Smith, M., Hickey, R., Malkas, L., and Pommier, Y. (2000). Conversion of topoisomerase I cleavage complexes on the leading strand of ribosomal DNA into 5'-phosphorylated DNA double-strand breaks by replication runoff. Mol. Cell. Biol. *20*, 3977–3987.

Sudimack, J., and Lee, R.J. (2000). Targeted drug delivery via the folate receptor. Adv. Drug Deliv. Rev. *41*, 147–162.

Suntres, Z.E. (2011). Liposomal Antioxidants for Protection against Oxidant-Induced Damage. J Toxicol *2011*, 152474.

Sun, X.L., Murphy, B.R., Li, Q.J., Gullapalli, S., Mackins, J., Jayaram, H.N., Srivastava, A., and Antony, A.C. (1995). Transduction of folate receptor cDNA into cervical carcinoma cells using recombinant adeno-

associated virions delays cell proliferation in vitro and in vivo. J. Clin. Invest. *96*, 1535–1547.

Tabatabaei, S., Shukohfar, A., Aghababazadeh, R., and Mirhaibibi, A. (2006). Experimental study of the synthesis and characterization of silica nanoparticles via sol-gel method. Journal of Physics: Conference Series. *26*, 371-374.

Takasuna, K., Hagiwara, T., Hirohashi, M., Kato, M., Nomura, M., Nagai, E., Yokoi, T., and Kamataki, T. (1996). Involvement of beta-glucuronidase in intestinal microflora in the intestinal toxicity of the antitumor camptothecin derivative irinotecan hydrochloride (CPT-11) in rats. Cancer Res. *56*, 3752–3757.

Tanizawa, A., Kohn, K.W., and Pommier, Y. (1993). Induction of cleavage in topoisomerase I c-DNA by topoisomerase I enzymes from calf thymus and wheat germ in the presence and absence of camptothecin. Nucleic Acids Res. *21*, 5157–5166.

Tian, F., Prina-Mello, A., Estrada, G., Beyerle, A., Moeller, W., Schulz, H., Kreyling, W., and Stoeger, T. (2008). A novel assay for the quantification of internalized nanoparticles in macrophages. Nanotoxicology. *4*, 232-242.

Tinkov, S., Bekeredjian, R., Winter, G., and Coester, C. (2009). Microbubbles as ultrasound triggered drug carriers. J Pharm Sci *98*, 1935–1961.

Toffoli, G., Cernigoi, C., Russo, A., Gallo, A., Bagnoli, M., and Boiocchi, M. (1997). Overexpression of folate binding protein in ovarian cancers. Int. J. Cancer *74*, 193–198.

Torchilin, V.P. (1998). Polymer-coated long-circulating microparticulate pharmaceuticals. J Microencapsul *15*, 1–19.

Torchilin, V.P. (2006). Multifunctional nanocarriers. Adv. Drug Deliv. Rev. *58*, 1532–1555.

Torchilin, V.P. (2007). Targeted pharmaceutical nanocarriers for cancer therapy and imaging. AAPS J *9*,

E128–E147.

Ulukan, H., and Swaan, P.W. (2002). Camptothecins: a review of their chemotherapeutic potential. Drugs *62*, 2039–2057.

Ungaro, F., d' Angelo, I., Coletta, C., d' Emmanuele di Villa Bianca, R., Sorrentino, R., Perfetto, B., Tufano, M.A., Miro, A., La Rotonda, M.I., and Quaglia, F. (2011). Dry powders based on PLGA nanoparticles for pulmonary delivery of antibiotics: Modulation of encapsulation efficiency, release rate and lung deposition pattern by hydrophilic polymers. Journal of Controlled Release: Official Journal of the Controlled Release Society.

Wagner, V., Dullaart, A., Bock, A.-K., and Zweck, A. (2006). The emerging nanomedicine landscape. Nat. Biotechnol. *24*, 1211–1217.

Wall, M.E., Wani, M.C., Cook, C.E., and Palmer, K.H. (1966). Plant antitumor agents, I: the isolation and

structure of camptothecin, a novel alkaloidal leukemia and tumor inhibitor from *Camptotheca acuminata*. J. Am. Chem. Soc. *88*, 3888-3890.

Watson, A. (2004). Getting the measure of nanotechnology. Science *306*, 1309–1310.

Weissleder, R., Elizondo, G., Wittenberg, J., Rabito, C.A., Bengele, H.H., and Josephson, L. (1990). Ultrasmall superparamagnetic iron oxide: characterization of a new class of contrast agents for MR imaging. Radiology *175*, 489–493.

Weitman, S.D., Frazier, K.M., and Kamen, B.A. (1994). The folate receptor in central nervous system malignancies of childhood. J. Neurooncol. *21*, 107–112.

Wheatley, M.A., and Lewandowski, J. (2010). Nano-sized ultrasound contrast agent: salting-out method. Mol Imaging *9*, 96–107.

Williamson, R. (2001). Prevention of birth defects: folic

acid. Biol Res Nurs *3*, 33–38.

Yang, L., Wold, M.S., Li, J.J., Kelly, T.J., and Liu, L.F. (1987). Roles of DNA topoisomerases in simian virus 40 DNA replication in vitro. Proc. Natl. Acad. Sci. U.S.A. *84*, 950–954.

Yokogawa, K., Nakashima, E., Ishizaki, J., Maeda, H., Nagano, T., and Ichimura, F. (1990). Relationships in the structure-tissue distribution of basic drugs in the rabbit. Pharm. Res. *7*, 691–696.

Zaman, M.B., Baral, T.N., Jakubek, Z.J., Zhang, J., Wu, X., Lai, E., Whitfield, D., and Yu, K. (2011). Single-domain antibody bioconjugated near-IR quantum dots for targeted cellular imaging of pancreatic cancer. J Nanosci Nanotechnol *11*, 3757–3763.

Zhang, H., Meng, L.-H., Zimonjic, D.B., Popescu, N.C., and Pommier, Y. (2004). Thirteen-exon-motif signature for vertebrate nuclear and mitochondrial type IB topoisomerases. Nucleic Acids Res. *32*, 2087–2092.

Zhang, L., Gu, F.X., Chan, J.M., Wang, A.Z., Langer, R.S., and Farokhzad, O.C. (2008). Nanoparticles in medicine: therapeutic applications and developments. Clin. Pharmacol. Ther. *83*, 761–769.

Zheng, S., Chang, S., Lu, J., Chen, Z., Xie, L., Nie, Y., He, B., Zou, S., and Gu, Z. (2011). Characterization of 9-nitrocamptothecin liposomes: anticancer properties and mechanisms on hepatocellular carcinoma in vitro and in vivo. PLoS ONE *6*, e21064.